THESIS FOR THE DEGREE OF DOCTOR OF PHILOSOPHY

Immobilization of Enzymes in Mesoporous Silica for the Conversion of CO_2 to Methanol

MILENE ZEZZI DO VALLE GOMES

Department of Chemistry and Chemical Engineering

CHALMERS UNIVERSITY OF TECHNOLOGY

Gothenburg, Sweden 2019

Immobilization of Enzymes in Mesoporous Silica for the Conversion of CO_2 to Methanol

MILENE ZEZZI DO VALLE GOMES
ISBN: 978-91-7905-186-0

Doktorsavhandlingar vid Chalmers Tekniska Högskola
Ny serie nr: 4653
ISSN:0346-718-X

Department of Chemistry and Chemical Engineering
Chalmers University of Technology
SE-412 96 Gothenburg
Sweden
Telephone + 46 (0)31-772 1000

Cover: Schematic illustration of the enzymes immobilized in the siliceous mesostructured cellular foams for the conversion of CO_2 to methanol.

Printed by:
Chalmers Reproservice
Gothenburg, Sweden 2019

“*Don't let anyone rob you of your imagination, your creativity, or your curiosity. It's your place in the world; it's your life. Go on and do all you can with it, and make it the life you want to live.”* - Mae Jemison, engineer, physician and former NASA astronaut. The first African American woman astronaut in space.

Immobilization of Enzymes in Mesoporous Silica for the Conversion of CO_2 to Methanol

MILENE ZEZZI DO VALLE GOMES
Department of Chemistry and Chemical Engineering
Chalmers University of Technology

ABSTRACT

Enzymes are powerful biomolecules able to catalyse chemical reactions under mild conditions and with high selectivity. However, their use in industrial processes is many times hindered due to their high costs and low stability. To overcome these problems the enzymes can be immobilized in an inert support material. The enzyme immobilization is also an interesting approach to increase enzyme activity, especially in the case of cascade reactions where more than one enzyme is involved.

One extremely relevant cascade reaction is the conversion of CO_2 to methanol that can be performed by three enzymes: formate dehydrogenase (FateDH) that converts CO_2 to formate; formaldehyde dehydrogenase (FaldDH) for the reduction of formate to formaldehyde; and alcohol dehydrogenase (ADH) that reduces formaldehyde to methanol. This reaction can help to mitigate the environmental impact caused by the high emissions of CO_2. However, the catalytic activity of the cascade reaction needs to be improved. In this work we investigate if an improvement can be achieved by the immobilization of the enzymes in a type of mesoporous silica particles (MPS), called siliceous mesostructured cellular foams (MCF), which physical and chemical properties can be specifically designed for the immobilization.

MCFs with different pores sizes containing the functional groups octyl (OC), mercaptopropyl (MP), chloromethyl (CM) or aminopropyl (AP) were synthesized. They were initially used to study the immobilization and reaction of each enzyme separately. However, the reaction performed by FateDH is thermodynamically unfavourable, thus it was necessary to add FaldDH in the system to drive the reaction towards the reduction pathway. The co-immobilization of these two enzymes in MCF-MP resulted in a specific activity of about 4 times higher than for the free enzymes in solution. Förster resonance energy transfer measurements suggested that the enzymes were in closer proximity inside this material which potentially contributed to the higher activity. For FaldDH, specifically, MCF with large pores were required for the enzyme to remain active upon immobilization and its activity was enhanced using MCF-MP. The catalytic activity of the last enzyme, ADH, was higher upon immobilization in MCF-OC. ADH showed to be sensitive to pressure, and high concentrations of formaldehyde were required to achieve high enzymatic activity. Combining the knowledge from those studies we co-immobilized the three enzymes in MCF-MP and obtained methanol yields about 4.5 times higher than with the free enzymes in solution.

One complementary study in this thesis was the comparison of two mesoporous silica materials, MCF and SBA-15, for the immobilization of ADH. From nitrogen sorption analysis we could observe that in MCF a larger fraction of the enzymes become immobilized inside the pores than on the outer surface in comparison to SBA-15, confirming that MCF is a good support material for this type of enzyme.

The findings of this work contribute to a better understanding of enzyme immobilization in MPS and the improvement of the rate of the reactions involved in the conversion of CO_2 to methanol.

Key words: *Immobilization, mesoporous silica, CO_2 reduction, biocatalysis, nitrogen sorption analysis*

LIST OF PUBLICATIONS

I. **Influence of operating conditions and immobilization on activity of alcohol dehydrogenase for the conversion of formaldehyde to methanol**
Milene Zezzi do Valle Gomes and Anders E.C. Palmqvist
New Journal of Chemistry, **2017**. 41(19): p. 11391-11397.

II. **Immobilization of formaldehyde dehydrogenase in tailored siliceous mesostructured cellular foams and evaluation of its activity for conversion of formate to formaldehyde**
Milene Zezzi do Valle Gomes and Anders E.C. Palmqvist
Colloids and Surfaces B: Biointerfaces, **2018**. 163: p. 41-46.

III. **Förster resonance energy transfer study of the improved biocatalytic conversion of CO_2 to formaldehyde by coimmobilization of enzymes in siliceous mesostructured cellular foams**
Pegah S. Nabavi Zadeh*, Milene Zezzi do Valle Gomes*, Björn Åkerman and Anders E.C. Palmqvist
ACS Catalysis, **2018**. 8(8): p. 7251-7260.
* Contributed equally as first authors

IV. **Improved biocatalytic cascade conversion of CO_2 to methanol by enzymes co-immobilized in tailored siliceous mesostructured cellular foams**
Milene Zezzi do Valle Gomes, Gerard Masdeu, Björn Åkerman and Anders E.C. Palmqvist
Manuscript

V. **Spatial distribution of enzymes immobilized in mesoporous silicas for biocatalysis**
Milene Zezzi do Valle Gomes*, Pegah S. Nabavi Zadeh*, Anders E.C. Palmqvist and Björn Åkerman
* Contributed equally as first authors
Under review in *ACS Applied Nano Materials*

CONTRIBUTION REPORT TO THE LISTED PUBLICATIONS

I. Designed the study, performed all the experimental work, analysed the data and wrote the manuscript.

II. Designed the study, performed all the experimental work, analysed the data and wrote the manuscript.

III. Designed the study together with Pegah Nabavi, performed and analysed all the experimental work related to the synthesis of silica, co-immobilization and activity of the enzymes. Wrote the manuscript together with Pegah Nabavi.

IV. Designed the study together with Gerard Masdeu, performed and analysed all the experimental work related to the synthesis of silica, co-immobilization and activity of the enzymes. Wrote the manuscript together with Gerard Masdeu.

V. Designed the study together with Pegah Nabavi, performed all the experimental work and analysis related to the synthesis of silica, enzyme immobilization and nitrogen sorption analysis. Wrote the manuscript together with Pegah Nabavi.

PUBLICATIONS NOT INCLUDED IN THIS THESIS

A. **Immobilisation on mesoporous silica and solvent rinsing improve the transesterification abilities of feruloyl esterases from Myceliophthora thermophila.**
Silvia Hüttner, Milene Zezzi Do Valle Gomes, Laura Lancu, Anders E.C. Palmqvist, Lisbeth Olsson
Bioresource Technology, **2017**. 239: p. 57-65.

B. **Measuring viscosity inside mesoporous silica using protein-bound molecular rotor probe**.
Pegah S. Nabavi Zadeh, Milene Zezzi do Valle Gomes, Maria Abrahamsson, Anders E.C. Palmqvist and Björn Åkerman
Physical Chemistry Chemical Physics, **2018**. 20(36): p. 23202-23213.

C. **Immobilization of bacterial feruloyl esterase on mesoporous silica particles and enhancement of synthetic activity by hydrophobic-modified surface.**
Sun Li Chong; Vânia Cardoso, Joana L. A. Brás; Milene Zezzi do Valle Gomes, Carlos M.G.A. Fontes and Lisbeth Olsson
Bioresource Technology, **2019**. 293: p. 122009.

TABLE OF CONTENTS

ABBREVIATIONS

ADH	Alcohol dehydrogenase
Cy3	Sulfo-Cyanine3 NHS ester
Cy5	Sulfo-Cyanine5 NHS ester
Cy7	Sulfo-Cyanine7 NHS ester
DOI	Degree of immobilization
ESEM	Environmental scanning electron microscopy
FaldDH	Formaldehyde dehydrogenase
FateDH	Formate dehydrogenase
GC-FID	Gas chromatography with flame ionization detector
MCF	Siliceous mesostructured cellular foams
MCF-AP	MCF functionalized with 3-aminopropyltriethoxysilane
MCF-Cl	MCF functionalized with chloromethyltriethoxysilane
MCF-MP	MCF functionalized with 3-mercaptopropyltrimethoxysilane
MCF-OC	MCF functionalized with octyltriethoxysilane
MPS	Mesoporous silica particles
NADH	Nicotinamide adenine dinucleotide
SBA-15	Santa Barbara amorphous-15 type ordered mesoporous silica
SEM	Scanning electron microscopy
TEM	Transmission electron microscopy
TEOS	Tetraethoxysilane
TGA	Thermogravimetric analysis
TMB	Trimethylbenzene
UV-Vis	Ultraviolet-visible spectroscopy

1. Introduction

The development of the societies with increase in population and standard of living has led to an explosive growth in the use of energy from fossil fuels [1, 2]. Advanced technologies, new methods and materials have been developed to diminish the human/industrial need for fossil fuels, but it is estimated that more than 85% of the energy used worldwide still remains derivate from non-renewable sources [3].

The fossil fuel combustion is responsible for high emissions of CO_2, which is the main greenhouse gas produced by human activity [2]. Since the industrial revolution, the concentration of this gas in the atmosphere of the Earth increased more than 30% and is the main cause of climate change and planetary temperature increase [1, 2, 4-6]. The global warming is considered a risk for future generations given the cumulative nature of CO_2. Therefore, sustained reduction of emissions has been found necessary [2, 7].

This issue is debated all around the world and some agreements were established to reduce CO_2 emissions (e.g. the Kyoto protocol in 1992). More recently the Paris Climate Accord has been implemented aiming 30% reduction in the CO_2 emissions worldwide from 2030 to 2050 [1, 8].

This ambitious goal can be active not only by replacing fossil fuels with renewable energy but also by recycling CO_2 [9-12].

Attempts have been done to recycle CO_2 to produce useful chemicals and fuels as methane, formate and methanol. Among those products, the production of methanol from CO_2 is the one receiving most attention, since methanol can be used as transportation fuel and raw material [9, 11, 13-15]. As a fuel, its combustion generates CO_2 that with the development of new technologies, could be recycled to produce renewable methanol in a sustainable and economical way [13]. Moreover, methanol can also replace fossil carbon in the production of ethylene and propylene that are widely used in the chemical industries [13].

CO_2 is, however, a very stable molecule (ΔG_f^o = -396 kJ·mol^{-1}) and its conversion to methanol is not thermodynamically favourable and requires high inputs of energy [4, 16, 17]. Thus, there are many challenges involved in developing sustainable routes to promoting this reaction, but the benefits from that would be enormous [1]. Therefore, extensive research has been done to reduce CO_2 to methanol involving different sustainable approaches, mainly using electrocatalysis, photocatalysis and biocatalysis [1, 4, 5, 10, 17-24].

In the electrocatalytic conversion of CO_2 to methanol, water is oxidised into molecular oxygen, with simultaneous reduction of CO_2 ($2CO_2 + 4H_2O \rightarrow 2CH_3OH + 3O_2$)[1, 24]. For the CO_2 reduction to occur, very negative overpotentials must be applied consuming more electrical energy and resulting in a system with very low selectivity. As example, copper based catalysts, commonly studied for such reactions, also give CO, formate, methane, ethylene, ethanol and hydrogen as by-products [1].

Photocatalytically, CO_2 reduction can be performed by using semiconductors such as titania (TiO_2) usually doped with metal or non-metal dopants in order to narrow its band gap and increase visible light utilization [9, 14, 20]. However, the best results found in the literature nowadays are still using UV light [14, 20]. To improve the photoreduction of CO_2 to methanol it is also necessary to optimize other experimental parameters, such as temperature, pressure, solvents, catalyst concentration and wavelength of the radiation [11, 14]. The adjustment of those parameters is particular for every photocatalytic system and quite complicated to carry out since many mechanisms competes with one another [14]. The major challenge, however, is related to the very low selectivity of the products formed. As in the electrochemical reduction of CO_2, the photocatalysis generates many other hydrocarbon products [14].

An interesting solution for the conversion of CO_2 to methanol is the biocatalysis performed by three enzymes in a cascade reaction: first, formate dehydrogenase (FateDH) converts CO_2 to formate, then formaldehyde dehydrogenase (FaldDH) reduces formate to formaldehyde and in the final step alcohol dehydrogenase (ADH) is used to convert formaldehyde to methanol [21]

(Figure 1). These three enzymes use the cofactor nicotinamide adenine dinucleotide (NADH) as the terminal electron donor [21].

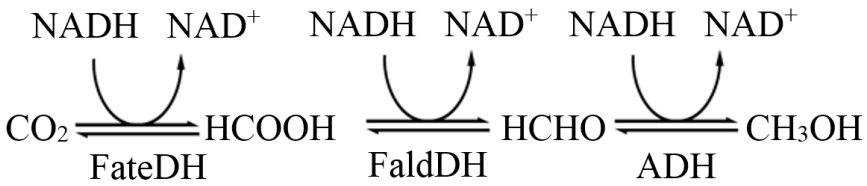

Figure 1. Conversion of CO_2 to methanol using a cascade reaction performed by formate dehydrogenase (FateDH), formaldehyde dehydrogenase (FaldDH) and alcohol dehydrogenase (ADH).

This is an interesting method to be investigated since enzymatic reactions have high selectivity and usually are performed under milder conditions than using chemical catalysts [17, 18].

The challenges in relation to this method lies in the fact that the reduction pathway is not the biological metabolic reaction performed by the enzymes. Therefore, the yields of methanol obtained are still not satisfactory. Furthermore, enzymes are known for being unstable and expensive. One way to overcome these problems is by immobilizing the enzymes in an inert support material [16, 21, 25, 26]. It can lead to higher yields of methanol and also higher enzyme stability and reusability, thus also contributing to decreasing the cost of the bioprocess [8, 21, 27].

As a support material for enzyme immobilization, mesoporous silica is the inorganic material most studied, thanks to the possibility of tailoring its morphology and chemical properties for the immobilization of each specific enzyme [28-31]. Also, the enzymes can be immobilized through physical adsorption, which is the simplest method to be used and no special conditions (e.g. salt or organic solvents) or equipment is required [28].

In this work, we investigated the bioconversion of CO_2 to methanol and studied the immobilization of the three dehydrogenases in tailored siliceous mesostructured cellular foams (MCF), a type of mesoporous silica that consists of large pores connected by narrow windows in a structure that resembles aerogels. The surface of the MCF was modified with the functional groups: aminopropyl, octyl, mercaptopropyl and chloromethyl, aiming at an improved interaction between enzymes and support. By doing so, we could investigate how the physical and chemical properties of the MCF affected the immobilization and activity of the enzymes. In **Paper 1** the focus was on the immobilization of alcohol dehydrogenase and how the operating conditions influence the activity of the enzyme. In **Paper 2** it was studied how the properties of the MCF directly impact the catalytic activity of formaldehyde dehydrogenase. In **Paper 3** formate dehydrogenase and formaldehyde dehydrogenase were co-immobilized in MCF and it was studied how the functional

groups present on the silica surface help to increase the yields of the reaction. Also, by using Förster resonance energy transfer (FRET) analysis it was possible to estimate the proximity of the immobilized enzymes. In **Paper 4** the co-immobilization of all the three enzymes and the improvement of the cascade reaction depending on the pore loading and method of immobilization were studied. In **Paper 5** it was investigated the spatial distribution of alcohol dehydrogenase immobilized in different types of mesoporous silica particles.

The overall objective of this work was to improve the bioconversion of CO_2 to methanol, by studying each biocatalytic reaction and developing an efficient immobilization strategy.

2. Background

2.1 Enzymes

Enzymes are biological macromolecules responsible for catalysing vital reactions in all living organisms. They are formed by long chains of amino-acids, which number, position and interactions affect the size, shape and function of the enzymes [32].

The amino acid sequence is considered the primary structure of the enzyme. The secondary structure is related to the interaction between the amino-acids which are in close proximity forming α-helix or β-sheets [32]. α-helix is formed by hydrogen bonds between the amino groups of the peptide backbone with the carboxyl groups of the amino-acid behind it [32]. In the β-sheet structure the hydrogen bonds are formed between parallel sections of the peptides chain [32]. The tertiary structure of the protein forms due to the interactions between parts of the proteins which are far apart in the primary structure [32]. In case of a multi chain protein, the spatial relation of the peptides in different chains forms the quaternary structure [32].

The three dimensional structure of the enzymes is, then, the result of many properties: the amino-acid sequence, the hydrogen bonding, the disulphide bonds, the hydrophobic interactions and

coulombic forces[32]. The three-dimensional structure leads to the formation of the active site, *i.e.* the specific location in the enzyme where the biocatalysis occurs. In the active site there are specific amino acids that can bind to the substrate molecules (reactants) through van der Waals forces, electrostatic or hydrophobic interactions, hydrogen and covalent bonds [33]. These interactions between enzyme and the substrate may induce conformational changes in the enzyme in order to optimize the binding of the substrate. During the catalysis two transient complexes (reaction intermediates) are formed by enzyme and substrate (ES), and enzyme and product (EP), respectively [33].

$$E + S \leftrightarrow ES \leftrightarrow EP \leftrightarrow E+P$$

Similar to homogeneous and heterogeneous catalysts, enzymes are able to increase the reaction rates without undergoing any permanent change. The biocatalysts accelerate the reaction rates by lowering the activation energy, *i.e.* the difference in energy between the ground state and the transition state (Figure 2). The thermodynamic equilibrium of the reaction, however, is not altered [33].

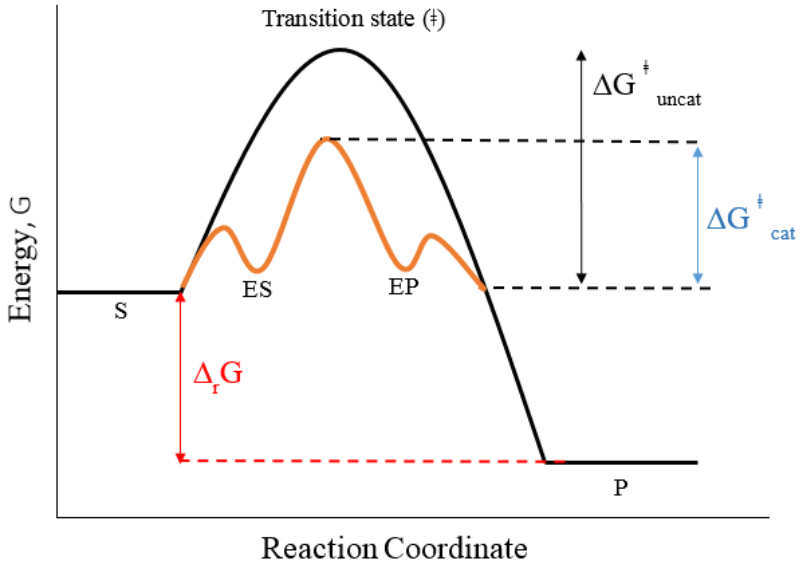

Figure 2. Reaction coordinate diagram of an uncatalysed (uncat) reaction compared with an enzyme catalysed (cat) reaction. *Redrawn from Principles of Biochemistry by Lehninger et al.* [33].

Enzymes are biocatalysts in very complex systems which requires them to have very high substrate specificity and reaction selectivity. This is highly desired and hard to be achieved in reactions using chemical catalysts[4, 17, 33].

2.2 Enzyme kinetics

The enzymatic kinetics were studied in 1913 by L. Michaelis and M.L. Menten [34]. They considered that the rate of the reaction is proportional to the concentration of the enzyme-substrate complex (ES).

The kinetics of an irreversible enzymatic reaction can be simplified in Figure 3.

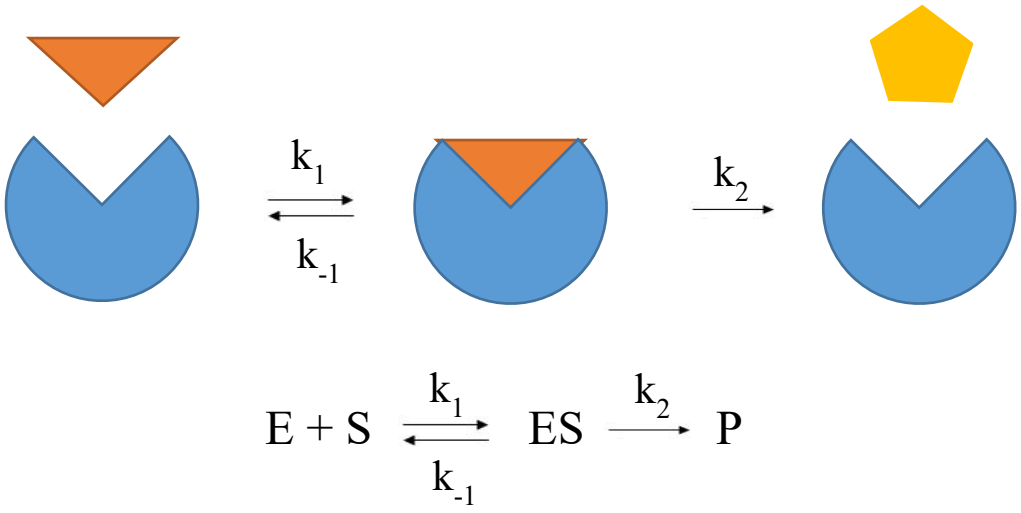

Figure 3. Illustration of the kinetics of an enzymatic reaction. The enzyme is denoted by *E*, the substrate by *S*, the enzyme-substrate complex by *ES* and the product by *P*. k_1, k_{-1} and k_2 are the reaction rates in the corresponding reaction steps.

Considering that the concentration of ES is constant over time (steady state), the following equations can be derived:

$$\frac{d[ES]}{dt} = ([E] \cdot [S]) \cdot k_1 - [ES] \cdot (k_{-1} + k_2) = 0 \qquad (1)$$

Equation 1 can be written as:

$$\frac{[E]\cdot[S]}{[ES]} = \frac{k_{-1}+k_2}{k_1} = K_M \qquad (2)$$

where K_m is the Michaelis-Menten constant. Its value shows the enzyme affinity for the substrate.

The slow step in equation 1 is the conversion of enzyme-substrate complex to product, so the velocity can be calculated as:

$$v = k_2 \cdot [ES] \qquad (3)$$

The maximum velocity is obtained when all the enzymes (E_T) form the complex ES:

$$v_{max} = k_2 \cdot [E_T] \qquad (4)$$

$$[E_T] = [E] + [ES] \qquad (5)$$

The Michaelis-Menten equation is obtained from equations 2,3,4 and 5.

$$v = \frac{v_{max}\,[S]}{K_m+[S]} \qquad (6)$$

From equation 6, K_m can be defined as the substrate concentration at half of the maximum velocity. A small K_m value indicates high affinity of the enzyme for the substrate. Hence, low substrate concentrations are needed for the maximum velocity to be reached. Contrary, high values of K_m indicates that the maximum velocity is only achieved using high substrate concentrations [35].

2.3 Parameters affecting enzyme activity

There are several parameters that can affect the enzyme activity, such as enzyme and substrate concentration, inhibitors, pH and temperature. Each of these factors are going to be discussed briefly in this chapter.

2.3.1 Enzyme and substrate concentration

According to Michaelis-Menten equation, the velocity of the enzymatic reaction increases by increasing substrate concentration (Equation 6) [35]. However, at a certain concentration of

substrate the reaction reaches the maximum velocity (V_{max}) possible for that concentration of enzyme, as can be seen in Figure 4.

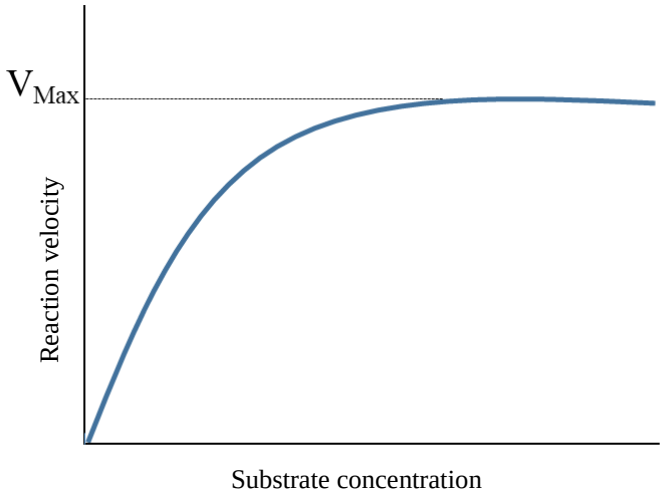

Figure 4. Effects of substrate concentration on the reaction rates.

To study the effect of enzyme concentration on the reaction rate, usually the substrate is used in excess, so the reaction is not limited by the substrate concentration. By increasing the enzyme concentration, the rate of the reaction tends to increase as exemplified in Figure 5 [35].

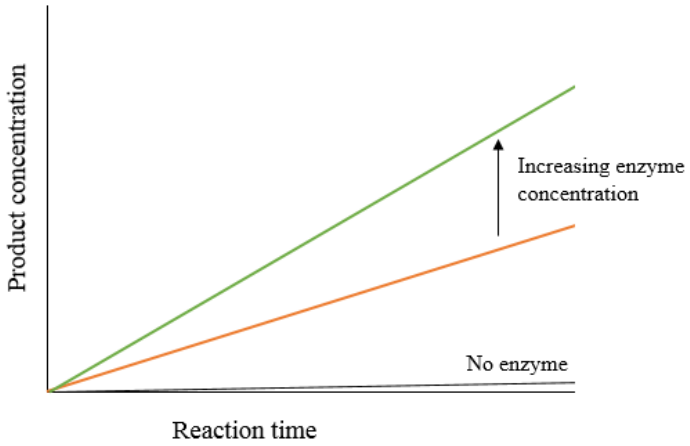

Figure 5. Effect of the enzyme concentration on the catalytic conversion rate (considering the reaction rate independent on the substrate concentration).

2.3.2 Enzyme inhibition

Some specific molecules can affect the enzyme by inhibiting its activity [35]. That can happen by the binding of these molecules to the active/regulatory site of the enzyme. The inhibition can be reversible or irreversible. While reversible inhibition usually regulates the flow through a metabolic pathway, irreversible inhibition leads to complete inactivation of the enzyme [36].

2.3.3 pH and temperature

The highest rate for the enzyme activity is usually found at one specific pH (pH_{opt}) and temperature (T_{opt}) (Figure 6) [37]. Those parameters are related to its application in nature. Some enzymes are even able to work in harsh conditions which are present in the environment where they are found [35, 36].

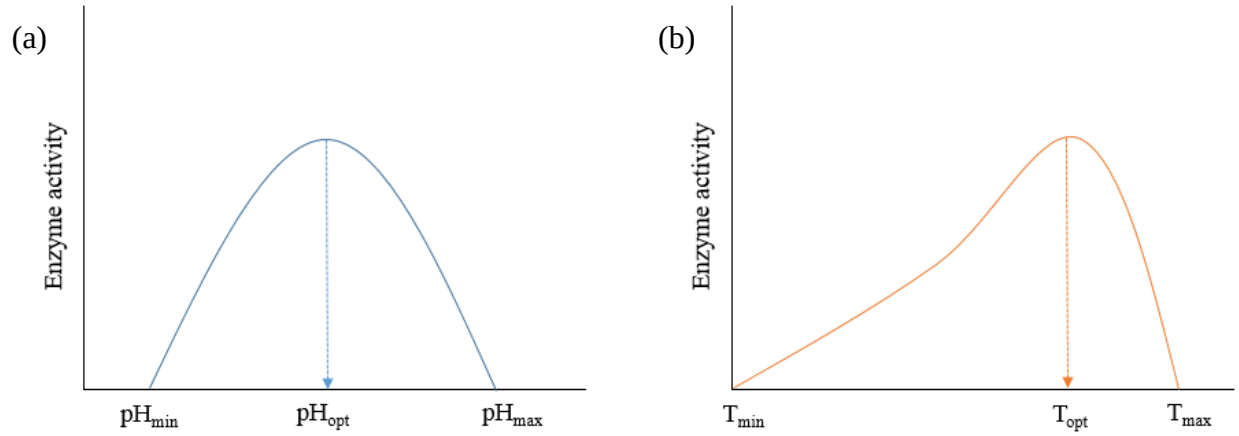

Figure 6. Schematic of typical (a) pH dependence of enzyme activity; (b) temperature dependence of enzyme activity.

For the reactions catalysed *in vitro*, the pH of the solution usually affects the protonation of the functional groups in the enzymes leading to changes in the net charge of the enzyme and its catalytic efficiency. The enzymes most affected by changes in pH are the ones which catalyze reactions involving proton transfer to/from protonic site(s) on the enzyme or substrate, and enzymes which mechanisms involve nucleophilic attack on a substrate atom and/or stabilization of a positively charged electrophilic intermediate [37].

It has been found that the catalytic activity of enzymes usually increases with increasing temperature, however, in temperatures higher than the optimum temperature (T_{opt}) the activity decreases rapidly due to irreversible thermal denaturation of the enzyme [37].

2.4 Oxidoreductases

Enzymes that catalyse oxidation-reduction reactions are called oxidoreductases. This means that they are able to catalyse the transfer of electrons from one molecule (the oxidant) to another (the reductant) reversibly. If the oxidised substrate is an oxygen donor, the enzyme is usually called dehydrogenase. If O_2 is the acceptor they are called oxidase [32].

In this thesis three oxidoreductase enzymes were used: formate dehydrogenase (FateDH), formaldehyde dehydrogenase (FaldDH) and alcohol dehydrogenase (ADH).

2.4.1 Formate dehydrogenase

FateDH (E.C.1.2.1.2) (Figure 7) from *Candida bondinii* consists of a homodimer of 42 kDa subunits, each one with an independent active site [38]. This enzyme reversibly converts CO_2 to formate using NADH as a cofactor. However, the reduction of CO_2 to formate is thermodynamic unfavourable (Table 2) [39]. In order to make the reduction reaction more favourable, NADH has to be used in excess, the product should be removed from solution rapidly after its formation and some studies also suggest that the use of enhanced pressure can be beneficial [18]. The optimum pH and temperature of the reducing reaction ($CO_2 \rightarrow$ formate) have been found to be in the range of pH 6.0 to 7.0 and 37 ºC, respectively [18].

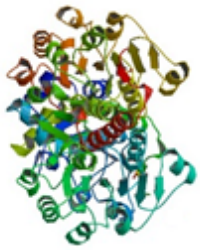

Figure 7. Formate dehydrogenase from *Candida bondinii* [40].

2.4.2 Formaldehyde dehydrogenase

FaldDH (E.C. 1.2.1.1) (Figure 8) is an enzyme obtained from *Pseudomonas* sp. This enzyme has a complex structure formed by a homotetramer of identical subunits, each one of them with 398 amino acid residues and 2 zinc ions. It has a global molecular mass of 170 kDa [41]. This oxidoreductase is used for the interconversion of formic acid to formaldehyde requiring NADH as a cofactor. FaldDH is also more efficient for the oxidation of formaldehyde, which reaction is thermodynamically favourable (Table 2) [42]. Kinetically it is not possible to compare the two pathways of this reaction, since K_m and V_{max} are difficult to obtain for the reduction of formic acid to formaldehyde. This is due to the fact that this enzyme is sensitive to substrate concentration and pH, *i.e*. it requires high concentrations of formic acid to be active, but in high concentrations of formic acid the pH of the solution becomes lower and the enzyme activity drops significantly [42]. In order to improve its activity as a reduction agent, high concentrations of the cofactor can be used. Its optimum pH for the forward reaction (formic acid → formaldehyde) is 6.5 and the optimum temperature is 37 ºC [18].

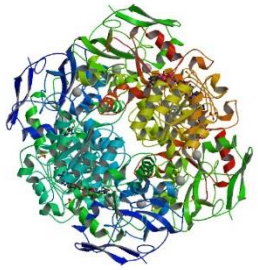

Figure 8. Formaldehyde dehydrogenase from *Pseudomonas* sp [41].

2.4.3 Alcohol dehydrogenase

ADH (E.C.1.1.1.1) (Figure 9) obtained from *Saccharomyces cerevisiae* is a homotetramer enzyme containing 347 amino acids in each subunit, with a molecular weight of about 141 kDa [43]. The catalytic domain in each subunit contains a zinc atom [43]. Differently from the other two enzymes, alcohol dehydrogenase is more efficient as a catalyst for the reduction reaction, *i.e.* the conversion of formaldehyde to methanol. It can be seen by the K_m and V_{max} values in Table 1 [42] and the negative $\Delta_r G'^{o}$ value in Table 2. The optimum conditions found for this reaction are the pH range of 5.5 to 7.0 and temperature of 25 ºC [18].

Figure 9. Alcohol dehydrogenase from *Saccharomyces cerevisiae* [43].

Table 1. Kinetic parameters of formate dehydrogenase, formaldehyde dehydrogenase and alcohol dehydrogenase. *

Enzyme	Reaction	K_m (mM)	V_{max} (mM·min^{-1})
Formate dehydrogenase (FateDH)	$CO_2 \rightarrow HCOO^-$ [a]	30-50	0.002
	$HCOO^- \rightarrow CO_2$	3.3	0.02
Formaldehyde dehydrogenase (FaldDH)	$HCOO^- \rightarrow HCHO$ [b]	-	-
	$HCHO \rightarrow HCOO$	0.06	0.01
Alcohol dehydrogenase (ADH)	$HCHO \rightarrow CH_3OH$	17.5	0.3
	$CH_3OH \rightarrow HCHO$	275	$0.5x10^{-3}$

*Data from Luo at al. [42], tris buffer pH 7; temperature = 23 ºC; NADH/NAD^+= 0.25 mM; FateDH= 50 µL (2.5 µg); FaldDH= 50 µL (100 µg); ADH 50 µL (50 µg); 2 mL substrate.
[a] Data from Ruschig et al.[44], CO_2 concentration varying from 0 to 15 mM, temperature = 20 ºC, pH 6.2. [b] values not possible to be determined.

Table 2. Gibbs free energy ($\Delta_rG'^o$) of the enzymatic reactions.*

Reaction	$\Delta_rG'^o$ (kJ·mol^{-1})
$CO_2 + NADH \leftrightarrow HCOO^- + NAD^+$	20.6
$HCOO^- + NADH + 2H^+ \leftrightarrow HCHO + NAD^+ + H_2O$	78.2
$HCHO + NADH + H^+ \leftrightarrow CH_3OH + NAD^+$	-96.2

* Data from Caspi et al. [39], at pH=7.3 and an ionic strength of 0.25.

2.5 Cofactor - NADH

The activity of many oxidoreductases is dependent on the cofactor NADH. This cofactor is the hydrogen source which is oxidized to NAD^+ stoichiometrically during the biocatalysis (Figure 10). The need of NADH is a drawback since it increases considerably the costs involved in enzymatic redox reactions [45, 46]. Specifically for the bioconversion of CO_2 to methanol this become even more significant since NADH is used in excess in order to drive the reactions towards the reduction pathway [18].

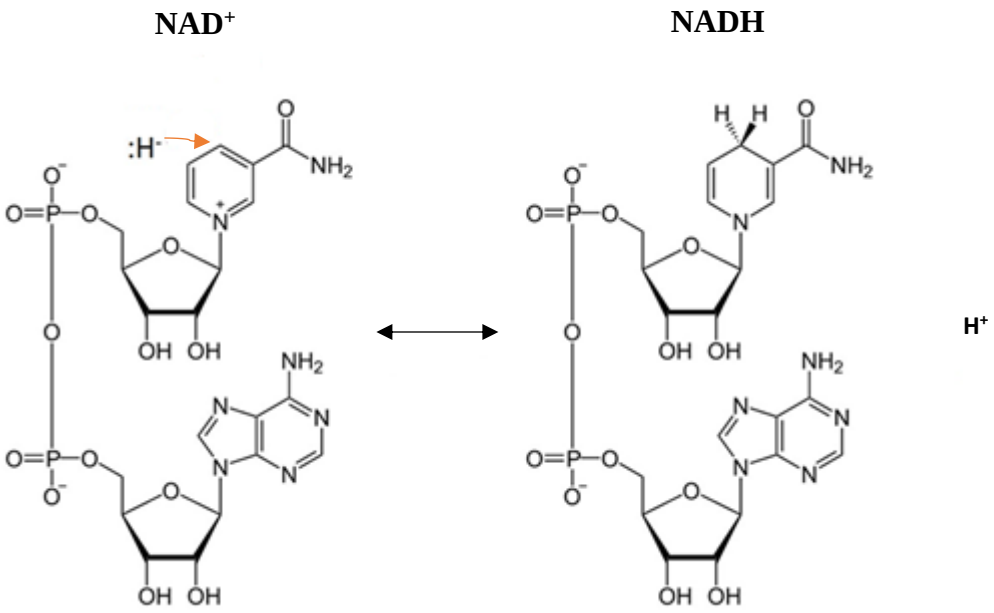

Figure 10. Redox reaction of the nicotinamide adenine dinucleotide.

For the use of NADH to become economically feasible, one possibility is the use of an in situ NADH regeneration system for reactions using NADH dependent oxidoreductases [46-48]. Such system is required to be inexpensive, stable over a long period of time and by-products formation should be negligible [49].

Electrocatalytic and photocatalytic regeneration systems usually demand a redox mediator as $[*Rh(bpy)_3]^{3+}$ that helps to decrease the overpotential (in the electrocatalysis) and increases the selectivity of the reaction for the production of 1,4-NADH, avoiding the formation of NAD dimers and 1,6-NADH that are inactive for the enzymes [47, 50]. For example, Huang et al. [50] reported high performance of graphitic carbon nitrate mesoporous spheres in regenerate NADH photocatalytically without a mediator system, but with poor 1,4 versus 1,6 selectivity. By adding the mediator, the selectivity increased significantly[50]. The need of the mediator can be, however, problematic when those regeneration systems are coupled with the enzymatic reaction since mutual inactivation of the mediator and enzyme may occur, reducing significantly the enzyme activity [47]. Attempts to overcome this problem involve the immobilization and compartmentalization of the enzymes, diminishing the direct interaction between the NADH dependent enzyme and the regenerator redox mediator [47]. Despite the challenges in developing of a photocatalytic regenerator system for NADH, this can be considered the most sustainable approach considering the inexhaustible character of sunlight[50].

The regeneration of NADH can also be performed enzymatically. Glucose-6-phosphate dehydrogenase oxidases D-Glucose-6-phosphate to D-Glucono-1,5-lactone-6-phosphate with the concomitant reduction of NAD^+ to NADH [49]. The disadvantages of the use of this enzymes is the expensive substrate and the rapid hydrolysis of D-Glucono-1,5-lactone-6-phosphate to 6-phosphogluconate which is difficult to separate from many reaction products [49]. A more suitable enzyme that can be used is Glucose dehydrogenase [18]. This enzyme converts β-D-Glucose, which is a cheaper substrate, to D-Glucono-1,5-lactone[49]. In some other systems, hydrogen dehydrogenase can be a good option since it oxidizes H_2 which is a cheap substrate[49]. However this enzyme has very poor stability, being very sensitive to oxygen [49]. Another option is the newly mutant phosphite dehydrogenase that was created to reduce NAD^+ (instead of $NADP^+$ reduced by the wild type enzyme), using the inexpensive phosphite as substrate[51].

These are just examples of many possible ways to regenerate NADH found in the literature [18, 47, 50-57]. The results are very promising and the combination of enzymatic redox reaction with simultaneous cofactor regeneration can potentially improve many biocatalytical systems [18, 47, 50-57].

2.6 Immobilization of enzymes

Biocatalytic processes can be applied industrially in many fields, such as for production of fine chemicals, fuels, pharmaceuticals and food [58]. Despite the advantages in the use of enzymes instead of chemical catalysts (high specificity and high catalytic efficiency under mild conditions), its application is rather limited due to high costs in production, instability and difficulties in reusability (enzymes are difficult to recover from the reaction media without losing activity) [59, 60]. These problems can be minimized by the immobilization of enzymes in an inert matrix [32]. The immobilization of enzymes can improve the enzyme stability since they become less susceptible to any inhibitors in the reaction media and also "protected" from extreme conditions which might be required in the catalysis; they can also be easily recycled leading to a great cost saving, and moreover, immobilization can lead to higher catalytic activity [30, 60, 61].

Many methods have been developed to immobilize enzymes, e.g. covalently binding the enzymes to a support; enzyme entrapment; cross-linking of enzymes; physical adsorption in solid supports (Figure 11) [29, 30, 60, 62, 63]. Each method presents advantages and disadvantages. Selection and optimization of the appropriate method for the enzyme immobilization are determinant for the enzymatic process to gain the benefits of the immobilization [29, 30, 60, 62, 63].

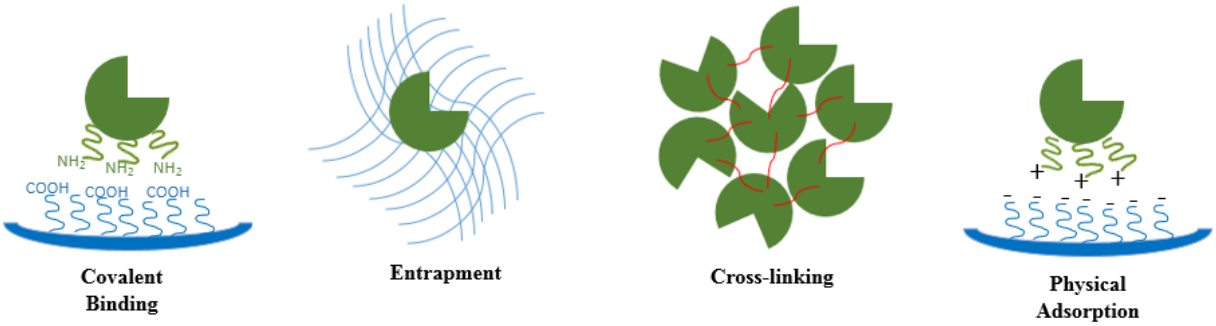

Figure 11. Illustration of the representative examples of covalent binding (amide bond formed by amine and carboxyl groups), entrapment, cross-linking of enzymes and physical adsorption (ionic interactions).

2.6.1 Covalent binding

Enzymes can be immobilized in an inert material through covalent binding. The host material is chosen depending on their properties of solubility, mechanical stability, hydrophilicity/hydrophobicity nature, surface area and functional groups. Common support carriers are agarose, cellulose and nanoparticles [59]. In this method of immobilization usually the support material is modified with reactive groups that bind to some specific functional groups (*i.e.* amines-, thiols-, phenolic-, imidazole- and carboxylic groups) present in the amino acids that are not essential for the enzymatic activity [59, 60, 64]. Since the enzyme is chemically bound to the support, it prevents the enzyme from being released during the reaction, which is one of the most positive aspects of this method [59, 64, 65]. However, the immobilization has to be carried out under conditions that do not lead to denaturation of the enzymes. Also, using *covalent binding* there is a risk that the structure of the enzyme becomes rigid and that the binding may induce conformational changes directly reducing the activity of the enzyme [59, 60, 63, 64].

2.6.2 Entrapment

Sol-gel materials and polymers can be used to immobilize enzymes via entrapment [60, 66]. In this method, the enzyme is added during the synthesis of the support material, resulting in the enzyme being encapsulated in its internal structure [59, 60, 62]. The main drawback of this method is the deactivation of the enzyme due to the conditions required in the synthesis of the support [59]. Then, in many cases the procedure needs to be modified in order to avoid the use of extreme conditions as high temperature and low pH [64]. However, even if the immobilization is performed

under mild conditions, it is not uncommon that entrapped enzymes have lower activity in comparison to the free enzyme, mostly due to problems related to mass transport restrictions [59].

2.6.3 Cross-linking

The immobilization of the enzymes can be done by intermolecular crosslinking forming enzymes aggregates (CLEAS) [32]. In this method there is no use of any support material. The enzymes form aggregates and precipitate by the addition of salts, organic solvents, acids or nonionic polymers [59, 60, 67]. Many enzymes are, however, sensitive to the coupling reagents necessary for the formation of CLEAS [60, 63]. Therefore, the conditions have to be carefully chosen and optimized to avoid losses in enzyme activity. The use of this method has shown to be advantageous mainly when the enzymatic reaction occurs in organic media [60].

2.6.4 Physical adsorption

Enzymes can be immobilized through physical adsorption in support carriers as mesoporous silica, carbon nanotubes and titania. This is considered one of the most simple and robust methods of immobilization [30, 63, 68]. The immobilization occurs due to van der Waals forces, hydrogen bonds, ionic- or hydrophobic interactions between the enzyme and the support material. If the enzymes interact with the support material through van der Waals forces, it is expected, however, that they would desorb from the support during the reaction since those are weak interactions. Electrostatic interactions, on the other hand, are the strongest forces that can be involved in the physical adsorption of the enzymes, avoiding enzyme leakage. Since there is no chemical bond between enzyme and support, it tend to not cause any conformational change in the enzyme and usually its activity is retained or even increased upon immobilization [30]. The major disadvantage of this method is the fact that enzymes may desorb more easily from the support material [32]. Thus, it requires the correct choice of the support for the adsorption to be stable and leakage avoided [29, 30].

2.7 Co-immobilization of enzymes

Enzymes can catalyse reactions that occur consecutively, *i.e.* cascade reactions where the product of the first reaction is the substrate for the following one, in a way that each step is dependent on the preceding reaction. In nature, enzymes that catalyse consecutive reactions are found close to each other, compartmentalized, in metabolons and scaffolds [69]. This compartmentalization is

extremely important for the high efficiency of the cascade system, since the reactions are usually substrate concentration dependent. Due to the compartmentalization, the concentration of the product of one reaction, called intermediate, will be found in higher concentrations in that specific location where it was produced [69]. Increasing the concentration of the intermediate potentially increases the activity of the enzyme in the subsequent reaction [69].

Compartmentalization also results in the enzymes being localized closer to each other than free in solution. It is much debated if this also contributes to higher activity or if the increase in the intermediate concentration is the main reason for the improvement in cascade reactions [69-71]. When the enzymes are localized in close proximity there is the possibility of substrate channelling, *i.e.* when the substrate is consumed without mixing completely with the bulk of the solution [72, 73]. It is estimated that there is a minimum distance between two active sites required for substrate channelling [72, 73]. There are two mechanisms possible for substrate channelling: one is the perfect channelling when the intermediate product is directly transfer to the second enzyme without diffusion to the bulk phase [74]. The other one is the proximity mechanism, where due to the fact that the enzymes are close, there is a higher probability of the second enzyme to consume the intermediate product before it goes to the bulk phase. In both situations the intermediate is hindered to diffuse in the bulk fluid by juxtaposition of the active sites and/or steric hindrance [74]. It is considered that substrate channelling can happen if the enzymes are not further away than 1 nm from each other [61]. However, some specific conditions as electrostatic guidance or compartmentalization can promote channelling at distances up to 10 nm [73]. For example, if the enzymes are co-localized in high concentrations the probability of the intermediate product from the first enzyme being consumed by the second enzyme increases significantly and substrate channelling can be achieved even if the active sites are further than 1 nm. This process is called "enzyme cluster-mediated channelling" [61, 70].

Compartmentalization of enzymes and substrate channelling can be achieved *in vitro* by co-immobilization of enzymes in an inert material, using DNA scaffolds or in systems that mimic the lipid matrix of biomembranes as artificial vesicles [61]. The success of the cascade reactions will depend on the orientation and distance of the active sites and the capability of the system to prevent the intermediate to diffuse to the bulk solution [61, 69].

2.8 Mesoporous silica as support carrier for enzymes

Mesoporous materials are excellent candidates for enzyme immobilization through physical adsorption. They can be synthesized with the pore diameters in the range of 2 to 50 nm, which matches the size of the enzymes and moreover, due to their high surface area and pore volume, the enzyme loading can be maximized to decrease the costs of the support carrier [29]. Ordered mesoporous silica, organosilica, carbons and titania are examples of mesoporous materials that

can be used for enzyme immobilization [28, 29, 68, 75]. Among them, mesoporous silica is the most widely studied since it is easily synthesized with cheap silica precursor (e.g. tetraethoxysilane (TEOS)) and by varying some synthesis parameters and the structure-direct agents (e.g. amphiphilic surfactants and biomacromolecules), a large variety of mesostructures can be obtained [29, 30]. Consequently, the physical properties of the material can be precisely tailored according to the properties of one specific enzyme [30, 76]. Furthermore, the silanol groups in the silica can be used to covalently attach specific organic groups (e.g. amines, thiol, and phenol) that can interact with the enzymes [31, 77]. The introduction of functional groups can result in lower leakage of enzymes during the reaction due to the increased enzyme-support interaction; it can also change the orientation of enzymes inside the pores so the active sites become more accessible to the reactants [30, 60, 63].

2.8.1 Pore size and morphology

The pore size and morphology are important physical parameters of the mesoporous silica that can affect the enzyme immobilization [27, 28, 68, 78]. A small variation in pore size can result either in enhanced or decreased enzyme activity and stability. It is presumed that the pores have to be big enough for the enzymes to diffuse inside of them, but it cannot be so large that it would increase the probability of enzyme leakage during the catalysis. The pores can neither be too tight that the enzyme loses its mobility and flexibility inside of them [30].

The morphology of the pore can affect the spatial distribution of enzymes through the particle and the diffusion of substrates and products [28]. Mesoporous silica with a hexagonal (SBA-15, MCM-41), cubic (KIT-6, SBA-16) and foam (mesostructured cellular foams-MCF) structures have been extensively studied for enzyme immobilization [28-30]. The cubic and foam structures can be considered advantageous for the immobilization due to the higher accessibility of the pores. In hexagonal structures the diffusion of the proteins into the long one-dimensional pores may be hindered due to enzymes that adsorb at the entrance of the pores thereby blocking it [30].

2.8.2 Surface functionalization

The functionalization of the mesoporous silica surface with organic groups can introduce different interactions between the enzyme and the support potentially increasing the adsorption stability [30]. However, the optimum physical interaction is not always predictable, due to the complexity of enzyme molecules. The enzyme-support interaction can involve amino acid residues in the enzyme outer surface and in the active site directly affecting the activity and stability of the enzyme [63, 79].

The surface functionalization can also be used to modify the hydrophilicity/hydrophobicity character of the support material. Hydrophilic surfaces are usually considered more suitable for the immobilization of water soluble enzymes, since the interaction between enzyme and a hydrophobic surface can lead to unfolding and inactivation of the protein [63, 80]. Still, for some specific enzymes the opposite effect is observed, and a higher activity is obtained depending on the degree of the surface hydrophobicity [30, 80, 81]. The specific reason for the gain in activity due to hydrophobic interactions is hard to be identified but it can be related to modifications in the secondary structure of the enzyme and also due to the fact that the stability of some enzymes inside of the cavities can be driven by an entropic effect in a way that inside of more hydrophobic pores the unfolded state loses more entropy then the folded state [81].

2.8.3 Particle size and morphology

Mesoporous silica can be synthesized with diverse particle morphology and size which can influence the enzyme immobilization. Rods and spheres are the most common morphologies of MPS [68]. Their sizes can vary significantly, influencing the ability of the enzymes to diffuse through the pores [68]. It is expected that in smaller particles there are more entrances to the pores and the enzymes can diffuse more easily occupying the core or length of the particle [82]. Furthermore, in smaller particles the enzymes tend to be more accessible to the substrates [82].

2.8.4 Siliceous mesostructured cellular foams

Siliceous mesostructured cellular foams (MCF) consist of ultra large mesopores, up to 40 nm in diameter connected via smaller windows of about 10 to 20 nm [83]. This cage like structure of the MCF, can be strategic for the enzyme immobilization since the pores are large to host high amounts of enzymes, but the pore entrance is narrower and therefore, leakage can be avoided [30]. Figure 12 shows an illustration of the immobilization of enzymes in MCFs.

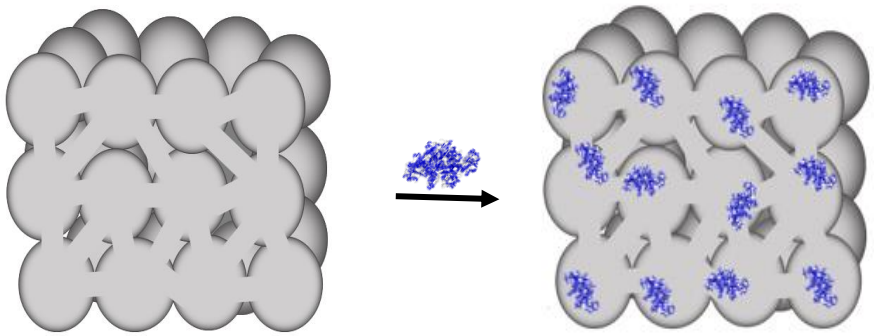

Figure 12. Schematic illustration of the enzymes immobilized inside of the MCF.

In the synthesis of MCF the largest pores are templated by oil in water microemulsion where trimethylbenzene (TMB) is the oil used as a swelling agent to increase the micelles of the triblock copolymer pluronic™ P123 ($EO_{20}PO_{70}EO_{20}$, Mw=5800), as shown in Figure 13.

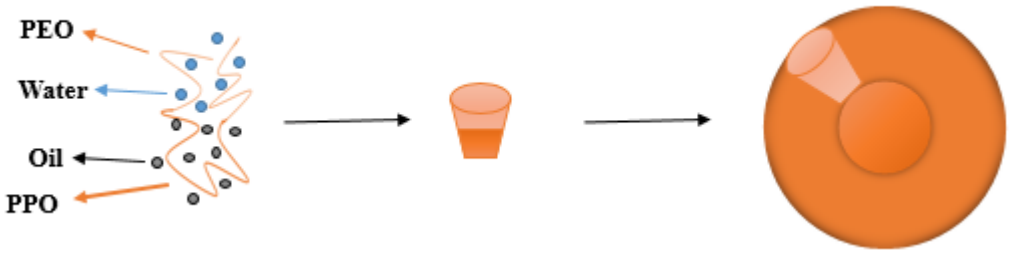

Figure 13. Formation of microemulsion droplets with the oil cores. The hydrophilic part of the triblock copolymer pluronic™ P123, polyethylene oxide (PEO) is partially hydrated whereas the oil solvates the hydrophobic groups, polypropylene oxide (PPO). Adapted from Lettow et al. [65].

The synthesis follows by the addition of TEOS, which hydrolyses and condenses forming the silica network around the template.

Hydrolysis:

$(RO)_3Si\text{-}OR + H_2O \leftrightarrow (RO)_3Si\text{-}OH + ROH$

Condensation:

$(RO)_3Si\text{-}OH + RO\text{-}Si(OR)_3 \leftrightarrow (RO)_3Si\text{-}O\text{-}SI(OR)_3 + ROH$

$(RO)_3Si\text{-}OH + HO\text{-}Si(RO)_3 \leftrightarrow (RO)_3Si\text{-}O\text{-}SI(OR)_3 + H_2O$

The material is then hydrothermally treated under static conditions. During this treatment the cells of silica agglomerate. The hydrophilic part of triblock copolymer pluronic™ P123, the polyethylene oxide chains (PEO), must be expelled from the cells, and this probably becomes the contact areas between them where windows are formed. By removing the template by calcination, the MCF is obtained in a structure that resembles aerogels. A schematic illustration of the process is shown in Figure 14.

The pore size and window size of the material can be tuned by modifying the aging temperature, the ratio of TMB/P123 or by adding NH_4F prior to the hydrothermal treatment [83, 84].

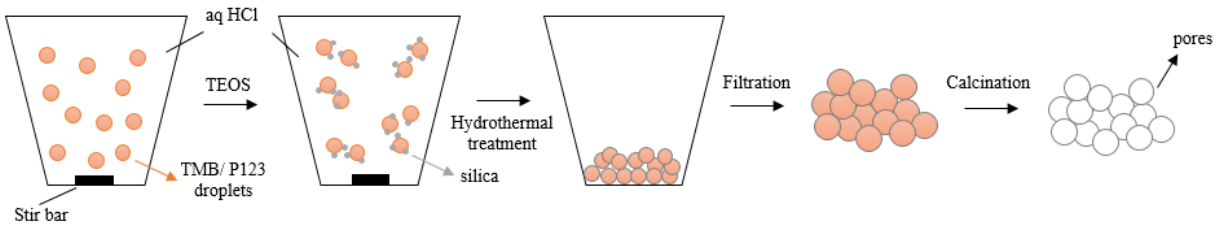

Figure 14. Schematic illustration of the stages of the MCF formation. Redrawn from Schmidt-Winkel et al. [83]

2.8.5 Ordered hexagonal mesoporous silica - SBA-15

In SBA-15 type of mesoporous particles, the pores are arranged in a hexagonal symmetry [85]. The synthesis procedure is very similar to MCF, however only pluronic™ P123 is used as template for the pore structure. During the synthesis of SBA-15, HCl is added to the reaction mixture dehydrating the hydrophilic PEO segments of the pluronic™ P123, whereas the ethanol released by the hydrolysis of TEOS swells the PPO chains. This leads to the formation of cylindrical micelles (Figure 15) [65]. The silica matrix is formed around those cylindrical micelles and the PEO chains can be deeply occluded within the silica walls creating microporosity in it [86]. By increasing the hydrothermal treatment temperature, the microporosity can be reduced [86].

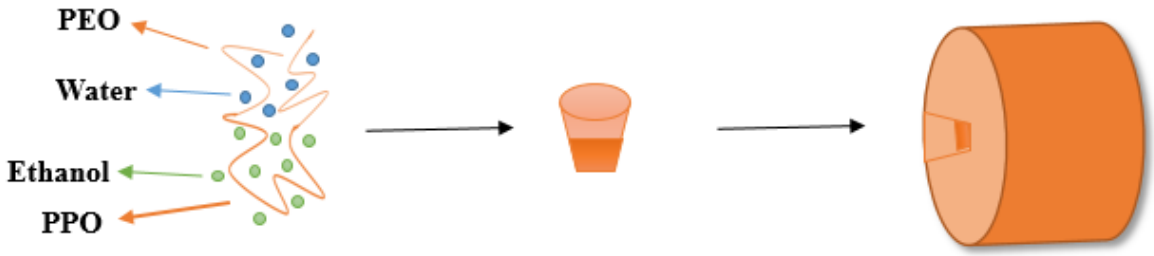

Figure 15. Formation of cylindrical micelles. HCl dehydrates hydrophilic PEO segments of the pluronic™ P123, and the ethanol released by the hydrolysis of TEOS swells the PPO chains. Adapted from Lettow et al. [65].

The particle shape and size and the pore diameter of SBA-15 can be tuned for the enzyme immobilization (Figure 16). The conventional synthesis procedure for SBA-15 produces rod-shaped particles. However, it is also possible to modify the method (e.g. addition of salt, use of static condition and low temperature in the synthesis) to obtain different particle shapes and sizes [68]. The pore sizes usually obtained varies between 2-10 nm and it is tuned by changing the temperature during hydrothermal treatment [87].

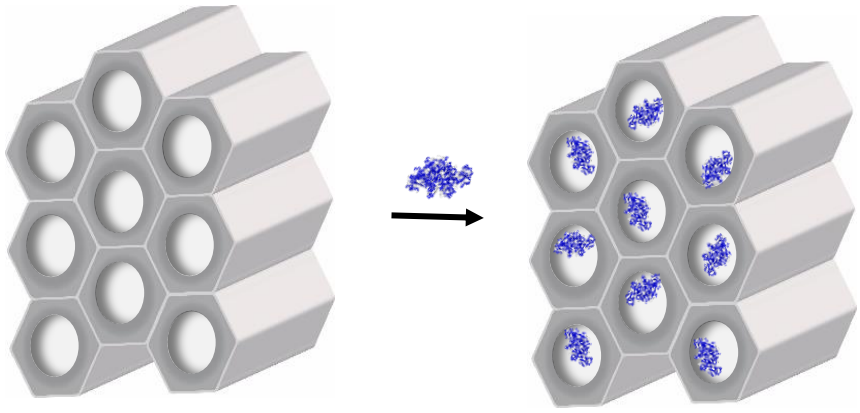

Figure 16. Schematic illustration of the enzymes immobilized inside of the SBA-15.

2.9 Application of immobilized enzymes for CO_2 reduction

The multi-enzymatic bioconversion of CO_2 to methanol is possible by reversing the biological pathway of the enzymes FateDH, FaldDH and ADH. Baskaya et al.[16] have demonstrated that the cascade reaction including the parallel oxidation of NADH is thermodynamically feasible, nevertheless the optimization of the reaction conditions is necessary for the production of high yields of methanol. The main attempt to achieve a better performance of the enzymatic system has been the immobilization of the biocatalysts [5, 17, 18, 21, 42, 54, 88-90].

The first work on the immobilization of the three dehydrogenases was performed by Obert and Dave in 1999 [21]. They co-immobilized the enzymes through entrapment in a sol-gel silica matrix resulting in higher methanol yields than obtained with the free enzymes in solution. Following this initial work, other studies have focused on the improvement of the support carrier. Organic-silica hybrid matrices, titania or more unconventional materials as hybrid microcapsules of catechol and gelatin [5, 17, 18, 88] have been used to co-immobilize the enzymes. However, no significant increase in the methanol production was observed. These results may be related to the fact that the enzymes were immobilized through entrapment. In this method the procedure for immobilization involves conditions, such as low or high pH, that may lead to damages in the three-dimensional structure of the enzyme. Moreover, the accessibility of the entrapped enzymes to the substrate can be hindered due to mass transfer resistance [64, 88].

In order to be able to improve the overall cascade reaction a better fundamental knowledge of each step of the system is needed. However, in the literature, there is only few studies considering the reactions performed by each enzyme independently. The main studies were performed by Cazelles at al. [18] and Luo et al.[42]. In their works are reported the different requirements for each enzyme in relation to pH, temperature and substrate concentration. Luo et al.[42] compared the kinetic values of each enzyme (Table 1) and suggested the use of a sequential reactor for the improvement of the cascade reaction [42].

Some reaction parameters can also be adjusted aiming for higher yields of methanol [18]. Cazelles at al. [18] observed that by using a closed reactor with 5 bars pressure the production of methanol can be nearly 3 orders of magnitude higher than in open systems [18]. It was also necessary to use NADH in excess to drive the reversible reactions towards reduction pathways[18]. This can be problematic considering the high cost of NADH. However, coupling the cascade reaction with an NADH regenerating system can overcome this problem and also increase the efficiency of the cascade reaction [18, 42, 54].

3. Theory and methodology

3.1 Methods

3.1.1 Synthesis of siliceous mesostructured cellular foams

Four MCFs (MCF1, MCF2, MCF3 and MCF4) were synthesized according to the procedure adapted from Schmidt-Winkel et al. [83] and Sridhar et al. [84]. Briefly, the triblock copolymer pluronic™ P123 was dissolved in 1.6 M HCl at room temperature and vigorous stirring followed by the addition of TMB. The temperature was raised to 40 ºC for 2 hours and then TEOS was added. After 20 hours at 40 ºC and vigorous stirring, NH_4F was added and the suspension was transferred to a stainless-steel autoclave with Teflon containers for 24 hours at 100 ºC. The sample was recovered by filtration and washed with distilled water. To remove the organic template the sample was calcined at 550 ºC for 8 hours with heating rate of 1 $ºC \cdot min^{-1}$. The mass ratio of TEOS to surfactant, and TMB to surfactant used were for MCF1: TMB/P123=1.5 and TEOS/P123=2.2; for MCF2: TMB/P123=2.0 and TEOS/P123=4.2, and for MCF3 and MCF4: TMB/P123=2.0 and TEOS/P123=2.0

MCF1 (pore size: 26.8 nm; window size: 10.5 nm) was synthesized aiming for pore sizes slightly bigger than the enzymes and was used in the immobilization of the three enzymes separately (paper

I, II and V). MCF2 (pore size: 32.9 nm; window size: 13 nm) was synthesized only for the immobilization of FaldDH (paper II) due to the large dimensions of this enzymes. MCF2 with larger pores and windows were obtained by increasing the TMB/P123 and TEOS/P123 ratios, respectively. MCF3 (pore size: 32.8 nm; window size: 11.3 nm) was used to co-immobilize FateDH and FaldDH (paper III). For the synthesis of this material and MCF4 the TMB/P123 ratio used was the same as for MCF2 aiming the formation of large mesopores, but the TEOS/P123 ratio was smaller to reduce the window size. MCF4 (pore size: 33.0 nm; window size: 10.9 nm was used to co-immobilize FateDH, FaldDH and ADH (paper IV);

3.1.2 Synthesis of SBA-15

SBA-15 particles were synthesized based on the method developed by Zhao et al. [76] and adapted by Gustafsson et al. [68, 87]. SBA-15 with 6.8 nm pore size (SBA-10-6.8) was obtained by first dissolving 4.0 g pluronic™ P123 in 120 ml of 2.0 M HCl and 30 ml of deionized water at 35 ºC, followed by the addition of 8.5 g of TEOS. The solution was stirred for 24 hours at the same temperature. After that, the sample was placed is stainless steel pressure autoclaves with Teflon containers and aged for 24 hours at 100 ºC. In the synthesis of SBA-15 with 10 nm pore size (SBA-15-10), 4.0 g pluronic™ P123 and 8 g of KH_2PO_4 were dissolved in 120 ml of 2.0 M HCl and 30 ml of deionized water at 35 ºC. After that, 8.5 g of TEOS was added and the sample was stirred for only 8 min and then kept under static condition for 24 hours at 35 ºC. Next, the sample was transferred to stainless steel pressure autoclave with Teflon container and aged for 24 hours at 140 ºC.

After aging, both materials were filtered, washed with deionized water and dried in air. The organic template was removed by calcination in air at 550 ºC for 8 hours (heating rate of 1 $ºC \cdot min^{-1}$).

SBA-15-6.8 and SBA-15-10 were used in paper V to investigate through nitrogen sorption analysis the immobilization and diffusion of ADH through the pores of the particles, considering that in SBA-15-6.8 the pores would be too small for the ADH to enter, and in SBA-15-10 the average pore size is on the border of admitting the ADH molecules. MCF1 was also used in this study (paper V) for the immobilization of ADH.

3.1.3 Surface functionalization

The surface of the MCFs was functionalized according to the procedure described by Russo et al. [31]. Prior to the reaction, 1 g of each MCF was dried at 120 ºC in vacuum oven for 4 h. The MCF was then mixed with a solution of chloromethyltriethoxysilane (CMTS), octyltriethoxysilane

(OCTS), 3-mercaptopropyltrimethoxysilane (MPTS) or 3-aminopropyl-triethoxysilane (APTS) in toluene. The mass ratio of MCF:organosilane used was 1:0.3. The sample was stirred for 10 min at room temperature and transferred to an autoclave at 100 ºC for 24 h. The functionalized MCFs were filtered, washed with toluene and dried at 120 ºC during 19 h. The final products were labelled as MCF (1,2,3or 4)-XX, where "XX" stands for the functional group in the surface (CM, OC, MP or AP) (Figure 17).

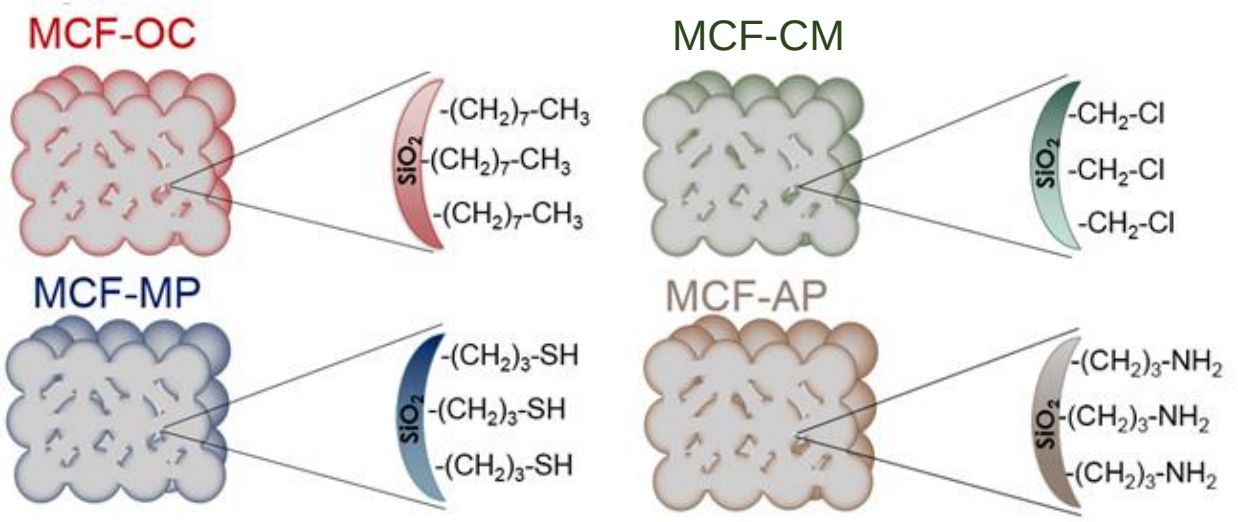

Figure 17. Schematic illustration of the functionalized MCFs.

3.1.4 Enzyme immobilization

The immobilizations of the individual enzyme in MCF or SBA-15 were performed by adding the MPS stock solution to a specified amount of enzyme depending on the target loading. The MPS stock solution and enzyme solutions were prepared in potassium phosphate buffer solution of pH 5.6 or pH 7.0 The samples were placed in a thermomixer at 37 ºC for FaldDH and FateDH, and 25 ºC for ADH under stirring.

The time used or necessary for the immobilization is an important parameter in terms of practical applications. To evaluate the maximum loading capability of each material, the immobilization was allowed for 24 h. However, for the preparation of the biocatalysts for the cascade reaction was used only the amount of time necessary to obtain the aimed protein loading and it varied for each enzyme. For FateDH the immobilization was allowed for 2 hours aiming for a protein loading of 150 $mg_{enzyme} \cdot g_{MCF}^{-1}$, for FaldDH, it was necessary with 3 hours for a protein loading of

150 $mg_{enzyme} \cdot g_{MCF}^{-1}$ and for ADH 1 hour was enough to obtain a protein loading of 130 $mg_{enzyme} \cdot g_{MCF}^{-1}$.

To study the spatial distribution of ADH in MCF and SBA-15, two pore loading were aimed, 150 and 300 $mg_{enzyme} \cdot g_{support}^{-1}$.

After the immobilization the samples were centrifuged and the concentration of enzyme that remained in the supernatant was estimated by measuring the UV-Vis absorbance of the supernatant at 280 nm using the extinction coefficient of each enzyme. The experiments were performed in triplicates with standard deviations lower than 5%.

The accomplished protein loadings (*PLD*), *i.e.* the amount of enzyme which was actually immobilized per amount of MPS, is estimated using equation 7. "W_{enz}" is the total weight of enzyme immobilized, "W_{MPS}" is the weight of MPS used for the immobilization. The pore filling (*Pf*) is the percentage of the pore volume of the MPSs that would be occupied after immobilization considering that all the enzymes are immobilized inside the pores, *i.e.* assuming that none of the proteins taken up are adsorbed to the external particle surface. It is calculated according to equation 8 where "V_{enz}" is the volume of the individual enzyme, "N_{enz}" is the number of enzymes, "V_{pore}" is the total volume of the pore before enzyme immobilization, "N_A" is Avogadro's number and "$M_{Wenzyme}$" the molecular weight of the enzyme. The degree of immobilization (DOI) is the fraction of enzyme that becomes immobilized (Equation 9). "W_{added}" is the total amount of enzyme that was added for the immobilization.

$$PLD = W_{enz} / W_{MPS} \quad (7)$$

$$Pf = V_{enz} N_{enz} / V_{pore} = V_{enz} N_A PLD / M_{Wenzyme} V_{Pore} \quad (8)$$

$$DOI = W_{enz} 100 / W_{added} \quad (9)$$

3.1.5 Co-immobilization of enzymes

An important part of the present work was to investigate the optimal strategy when two or three types of enzymes were immobilized together. These immobilization studies were all performed in in phosphate buffer pH 5.6, at 37 ºC using a thermomixer at 900 rpm.

3.1.5.1 Co-immobilization of FateDH and FaldDH

FateDH and FaldDH were co-immobilized in the MCF3 and MCF3-MP using three different enzyme mass ratios for FateDH:FaldDH of 1:1, 1:3 and 1:15. Two methods were tested: (1) Simultaneous co-immobilization, where 10 µl of FateDH at 2, 10 or 30 $mg \cdot ml^{-1}$ and 20 µl of FaldDH at 15 $mg \cdot ml^{-1}$ were added at the same time to the appropriate volume of MCF3 or MCF3-MP (20 $mg \cdot ml^{-1}$) to give a total amount of added enzyme of 150 $mg_{enzymes} \cdot g_{particles}^{-1}$. The immobilization was allowed for 4 hours in a thermomixer at 37 ºC and 900 rpm; (2) Sequential co-immobilization in which initially the 10 µl of FateDH at 2, 10 or 30 $mg \cdot ml^{-1}$ was mixed with the same volumes of MCF or MCF-MP (20 $mg \cdot ml^{-1}$) and agitated for 2 hours in a thermomixer at 37 ºC. Next, 20 µl of FaldDH at 15 $mg \cdot ml^{-1}$ was added to the pre-immobilized FateDH sample and the immobilization continued for another 4 hours under the same conditions. Afterwards, the samples were centrifuged and washed three times with 100 mM phosphate buffer and pH 6.5.

3.1.5.2 Co-immobilization of FateDH, FaldDH and ADH

The three enzymes, FateDH, FaldDH and ADH, were co-immobilized in MCF-MP following a sequential addition: (a) 2-hour incubation of the first enzyme together with MCF-MP, (b) addition of the second enzyme to the mixture, and incubation for 2 h, and (c) final addition of the third enzyme for 2 extra hours.

The enzymes were co-immobilized in two different orders: first according to the reaction order, FateDH→FaldDH→ADH, and secondly, according to their size, from the smallest to the biggest, FateDH→ADH→FaldDH.

For the immobilizations, the enzymes, FateDH (0.05 $mg \cdot ml^{-1}$), FaldDH (0.75 $mg \cdot ml^{-1}$) and ADH (3.75 $mg \cdot ml^{-1}$) were mixed with appropriated amounts of MCF-MP stock solution (0.05 $g \cdot ml^{-1}$) aiming for protein loadings of 50 or 150 $mg_{enzymes} \cdot g_{support}^{-1}$. After the immobilization the samples were centrifuged and washed with 100 mM phosphate buffer at pH 6.5.

3.1.6 Enzyme activity

The conditions used for measuring the catalytic activity of each enzyme separately (with or without particles) are shown in Table 3. For the reactions performed under pressure and CO_2 atmosphere a closed reactor was used. The other reactions were carried out in Eppendorf tubes placed in a thermomixer. In all the cases the samples were gently stirred during the reactions.

The specific activity of each independent enzyme was estimated by following the consumption of NADH during the reactions. The initial and final concentration of NADH was calculated by measuring the absorbance of the solution at 340 nm. As baseline reference, the UV-vis absorbance procedure was carried out under the same conditions, but without the enzymes. Samples containing immobilized enzymes were centrifuged and the supernatant was used to quantify the remaining NADH in solution. Experiments were performed in triplicates.

Table 3. Conditions used to evaluate the catalytic activity of each enzyme.

Enzyme	Enzyme conc. ($mg \cdot ml^{-1}$)	Substrate	Substrate conc. (mM)	NADH conc. (mM)	Time (min)	Temperature (ºC)	Pressure* (bars)
FateDH	1.5	$KHCO_3$[#]	3	1.5	30	37	no
FateDH	1.5	$KHCO_3$[#]	50	100	60	37	5
FaldDH	1.5	HCOONa	3	1.5	30	37	no
FaldDH	$1.5x10^{-1}$	HCOONa	50	100	60	37	5
ADH	$4.5x10^{-3}$	HCHO	3	1.5	30	25	no
ADH	$7.5x10^{-1}$	HCHO	50	100	60	25	5

*under CO_2 atmosphere.

[#] $KHCO_3$ was used instead of bubbling CO_2 for a better reproducibility of the reaction.

For the cascade reactions using FateDH and FaldDH the activity tests were performed by using different concentrations of FateDH (0.1, 0.5 or 1.5 $mg \cdot ml^{-1}$) with fixed amount of FaldDH (1.5 $mg \cdot ml^{-1}$) free in solution or co-immobilized. The enzymes were mixed with NADH (100 mM), and $KHCO_3$ (200 mM). $KHCO_3$ was used instead of bubbling CO_2 for a better reproducibility of the reaction. The reactions were performed in a closed reactor at pH 6.5 and 37 ºC, under CO_2 atmosphere at 5 bars pressure for 1 hour under stirring.

In the conversion of CO_2 to methanol using the three enzymes, FateDH, FaldDH and ADH, free or immobilized, the reactions were performed by mixing FateDH (0.05 $mg \cdot ml^{-1}$), FaldDH (0.75 $mg \cdot ml^{-1}$), ADH (3.75 $mg \cdot ml^{-1}$), NADH (100 mM), and $KHCO_3$ (200 mM). The solutions were prepared using 100 mM phosphate buffer at pH 6.5. The reactions were performed in a closed reactor at pH 6.5 and 37 ºC, under CO_2 atmosphere at 5 bars pressure for 1 hour under stirring.

3.1.7 Nash method for formaldehyde quantification

The amount of formaldehyde produced in the cascade reaction using FateDH and FaldDH, was quantified using Nash's method [91]. Nash's reagent was produced by mixing 25 g of ammonium acetate, 2.1 ml of acetic acid and 0.2 ml of acetyl acetone to a total volume of 100 ml in water. After the enzymatic cascade reaction, equal amounts of Nash's reagent and the reaction product were mixed for 1 h at 37 ºC. The formaldehyde produced during the enzymatic catalysis

reacts with the NASH's reagent forming diacetyldihydrolutidine which absorbs light at 414 nm (Figure 18) [91]. Hence, the amount of formaldehyde obtained was quantified indirectly by measuring the absorbance of the final sample using UV-vis spectroscopy.

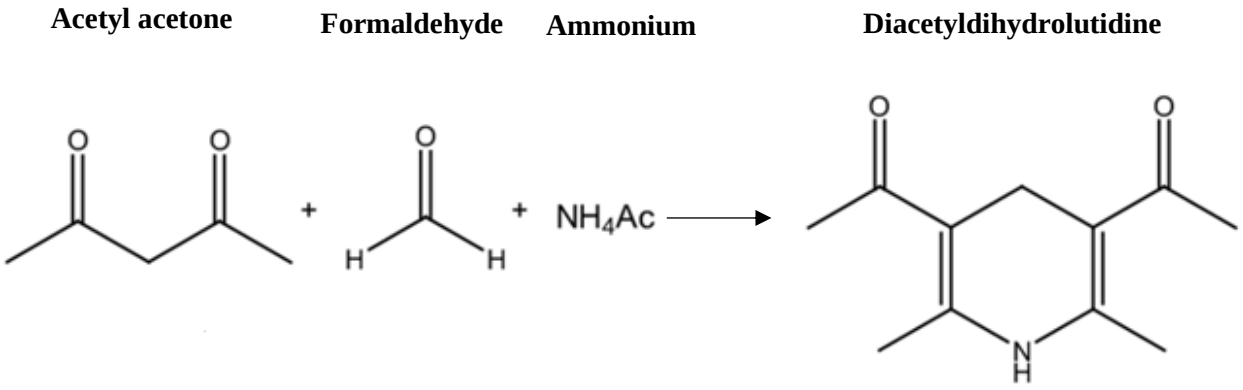

Figure 18. Reaction of formaldehyde with Nash's reagent.

3.1.8 Leakage tests

Enzymes leakage tests were performed under similar conditions as the activity tests but without adding NADH. The samples were then centrifuged and the enzymes that leached out from the MCF were quantified by UV-Vis absorbance of the supernatant at 280 nm.

3.2 Analytical techniques

The mesoporous silica particles were characterized by nitrogen sorption analysis, transmission electron microscopy (TEM), environmental scanning electron microscopy (ESEM) and thermogravimetric analysis (TGA). The concentrations of enzymes, NADH and diacetyldihydrolutidine (from the reaction of formaldehyde with Nash's reagent) were determined using UV-vis spectroscopy. To estimate the distance between co-immobilized enzymes Förster resonance energy transfer (FRET) was used. Gas chromatography with flame ionization detector (GC-FID) was used to quantify methanol.

3.2.1 Nitrogen sorption analysis

Gas adsorption is used to characterize the physical properties of mesoporous materials such as average pore size, specific pore volume and specific surface area. During the experiments an adsorbate physisorb on the material's surface, condensing to a liquid-like phase at a certain pressure (p), which is lower than the saturation pressure (p_0). At low relative pressures (p/p_0) one monolayer of adsorbed gas is formed on the surface of the material. By increasing the pressure step-wise, multi-layers of adsorbed gas are formed until reaching a critical film thickness. Then, the molecules get in close contact with each other and collapse into a thermodynamically lower energy state. A plateau region is observed when the pores are completely filled. Upon subsequent lowering the pressure, for mesoporous materials the molecules with low energy do not tend to desorb as readily, so the pore evaporation occurs at lower relative pressures than the pore condensation, thus resulting in a hysteresis of the sorption. The hysteresis loop closes when just a monolayer film is still adsorbed on the surface [92]. An example of an isotherm for mesoporous materials is shown in Figure 19.

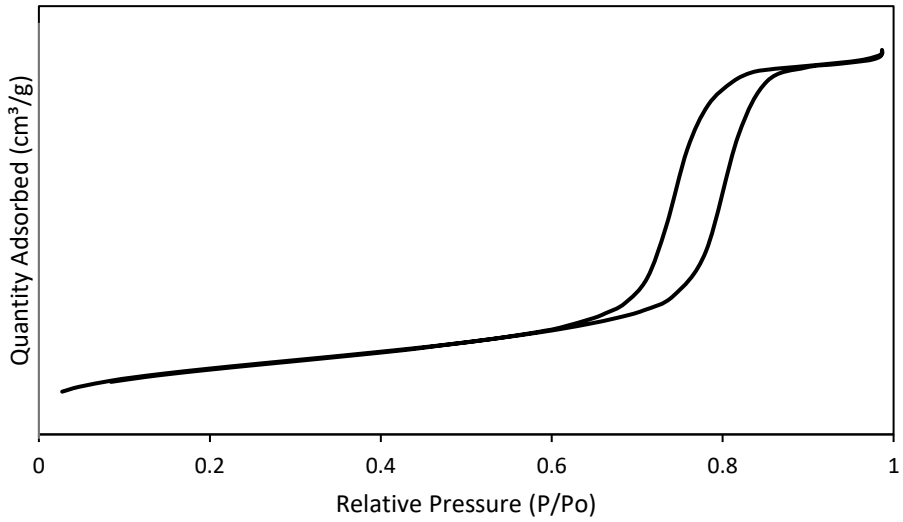

Figure 19. Example of isotherm and hysteresis loop typical of mesoporous materials.

To calculate the surface area of the materials, the BET (Brunauer-Emmett-Teller) theory is used [93]. It considers that the adsorbate adsorb first in the more energetic sites and the average residence time of a physically adsorbed molecule is longer on the higher-energy sites. As the pressure increases a close packed arrangement is expected, resulting in the formation of a

monolayer of the adsorbed gas. It happens at low relative pressures and therefore, the BET theory is applied only for values of p/p_0 varying from 0.05 to 0.35 [94].

MCFs possess "ink bottle" pores, which means that the large spherical pores are connected via smaller "necks" or windows. To determine the pore and window size in this material the BdB(Broekhoff - deBoer) - FHH(Frenkel - Halsey - Hill) method is applied [95].

The BdB method is based on Kelvin equation modified by Cohan (10), where "*f*" is a factor that is determined by the Laplace curvature of the meniscus, "γ" is the surface tension of the adsorbate, "*r*" is the pore diameter, and "*t*" is the thickness of the adsorbed layer [96].

$$\ln(P/P_0) = \frac{f\gamma V_m}{RT(r-t)} \qquad (10)$$

However, in this equation the effect of the curvature of the pore wall on the thickness of the adsorbed gas layer is neglected. In the BdB theory, this parameter is included in the equation as follows:

$$\ln(P/P_0) - \mathrm{F(t)} = \frac{f\gamma V_m}{RT(r-t)} \qquad (11)$$

To determine "*F(t)*" according to the BdB method is rather complicated, but it can be replaced by Hill's approximation (equation 12), where "α" is an empirical constant determined by the adsorbent and the adsorbate.

$$F(t) = \frac{\alpha}{t^3} \qquad (12)$$

The main equation for the modified BdB method, then called the BdB-FHH method, is shown in equation 13.

$$\ln(P/P_0) - \frac{\alpha}{t^3} = \frac{f\gamma V_m}{RT(r-t)} \qquad (13)$$

The adsorption isotherms are used to calculate the pore size distribution, whereas desorption branches are used to determine the mean window size [95].

The Barrett, Joyner, and Halenda (BJH) method [97] can be used to determine the pore size of SBA-15 [98]. This method assumes that all the pores have cylindrical shape, so the simple Kelvin equation (equation 10) can be used, considering "*f*" equals to 2 [99].

In BJH theory for each step in the isotherm the difference in the amount of adsorbate that become adsorbed represents the pore volume filled or emptied [99].

The pore volume of MPS is determined using the total liquid volume adsorbed at relative pressure $p/p_0 = 0.99$ [99].

Physisorption measurements were performed with nitrogen as adsorbate using a TriStar 3000 instrument from Micromeritics Instrument Corporation. The samples were outgassed for at least 8 hours at 180 ºC for the non-functionalized MCFs, and 120 ºC for the surface functionalized MCFs. For the samples containing immobilized enzymes, prior to the measurements they were freeze dried and then outgassed for 30 hours at 50 ºC.

3.2.2 Transmission electron microscopy

TEM is a unique tool in characterizing the structure of a material. It is an advanced microscopy technique where a beam of high energy (>100 keV) electrons is transmitted under vacuum through an ultra-thin film. The electrons interact with the specimen and an image is formed by objective lens situated below the sample, which is magnified by projector lens and focused in an imaging device (Figure 20). TEM is analogous to an optical microscope, where an electron source is used instead of a light source. Since the wavelength of electrons is much smaller than that of light, a very high magnification up to 10^6, with a resolution in the range of 1 Å can be achieved by TEM [100]. In this thesis, TEM images were obtained using Zeiss Leo 912 AB OMEGA.

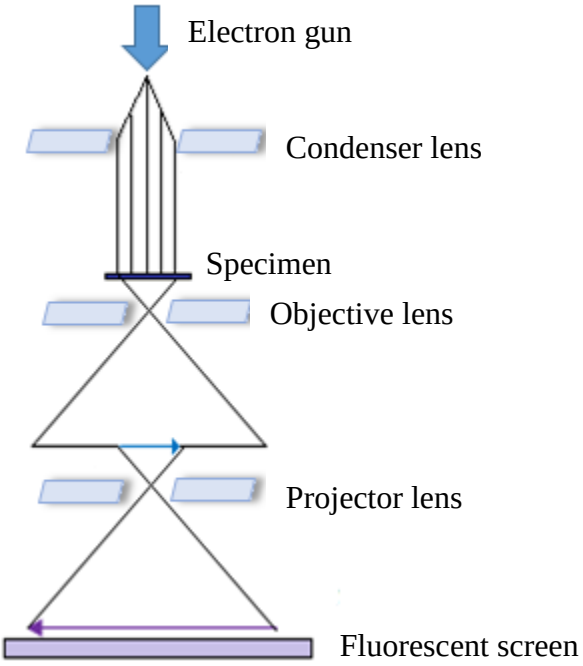

Figure 20. Basic features of transmission electron microscopy.

3.2.3 Environmental scanning electron microscopy

Environmental scanning electron microscopy (ESEM) is a useful microscopy technique where non-conductive surfaces can be analyzed without any preparation. Similar to scanning electron microscopy (SEM), ESEM employs an electron beam which is scanned over the specimen producing signals due to the interaction of the electrons with the sample. Secondary electrons (SE) and backscattered electrons (BSE) are detected and an image is constructed from the signal by a viewing system, revealing information about the nano- and microscale sample topography[101]. In ESEM, however, the samples are not analyzed in vacuum but in a gaseous environment at different pressure, temperature and composition in the specimen chamber. In ESEM the specimen chamber is isolated from the upper and lower portion of the vacuum column by multiple Pressure Limiting Apertures (PLA) [101]. Due to the gaseous environment a special detector called Gaseous Detector Device (GDD) has to be used [101]. The GDD employs an electrode with a voltage to several hundred volts which accelerate the emitted SE which collides with the gas molecules producing a cascade of electrons (Figure 21) [101]. This amplifies the signal before it reaches the detector. During this cascade process positive ions are produced which compensates the negative charge build up, allowing the imaging of non-conductive samples [101].

In this project the ESEM was carried out on a FEI Quanta 200 FEG and the images obtained used to analyze the morphologies of the synthesized MCF1 and MCF2.

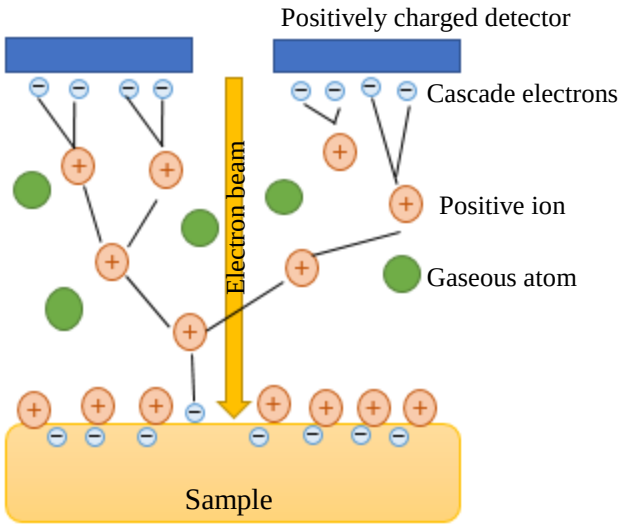

Figure 21. Cascade amplification process in ESEM.

3.2.4 Thermogravimetric analysis

TGA measures the weight loss of a sample as a function of time/temperature and atmosphere. This technique was used in this thesis to confirm that the organic groups were chemically bound to the silica surface (see Figure 17). Also, by knowing the weight loss measured for each functionalized MCF, it was possible to estimate the surface loading and the surface density according to equations 14 and 15, respectively. W_{loss}" is the weight loss per 100g of MCF, "N_A" is Avogadro's number and "$M_{W,\ ligand}$" is the molecular weight of the ligand. The remaining silanol groups in the surface ($R_{Si\text{-}OH}$) was estimated using Eq. (16), considering that each organosilane reacts with up to 2 silanol groups in the silica surface [53]. "D_{Si-OH}" is the average silanol surface density (5.2 OH·nm^{-2}) for amorphous silica [102]. TGA was carried out on a TGA/DSC 3+ instrument from Mettler Toledo, with heating rate of 10 ºC·min^{-1} under a N_2 flow of 50 ml·min^{-1}.

$$N_S = W_{loss}/(100g\ MCF\ x\ M_W\ ligand) \quad (14)$$

$$D = N_A \cdot N_S/Surface\ area \quad (15)$$

$$R_{Si-OH} = D_{Si-OH} - (2\ x\ D) \quad (16)$$

3.2.5 UV-Vis spectroscopy

UV-Vis spectroscopy measures the absorbance of analytes in the ultraviolet and visible region. The amount of light absorbed is directly proportional to the concentration ("c") of the absorbing species according to the Bouguer-Lambert-Beer law:

$$A = log\frac{I_0}{I} = \varepsilon cL \quad (17)$$

In equation 17, "*A*" is the absorbance, "I_o" is the intensity of the monochromatic light entering the sample, "*I*" is the intensity of the monochromatic light emerging from the sample, "*L*" is the path length through the solution and "ε" is the extinction coefficient. The extinction coefficient is a quantity characteristic of each substance which also depends on the wavelength (nm).

UV-Vis spectroscopy is an easy, rapid and straightforward method to quantify proteins thanks to the presence of the amino acid residues tyrosine and tryptophan which absorb at 280 nm. In this work, UV-Vis spectroscopy was used to determine enzyme concentration and to quantify the amount of immobilized enzyme indirectly, by measuring the amount of enzymes that remained in the supernatant after immobilization, using the extinction coefficient $E^{1\%}$ (values for 1%

(= 1g/100mL) solutions measured in a 1 cm cuvette) of each enzyme. $E^{1\%}$= 15.9 for FateDH; $E^{1\%}$ = 10.0 for FaldDH, $E^{1\%}$ = 14.6 for ADH, as provided by the supplier). UV-Vis spectroscopy was also used to quantify the NADH at 340 nm before and after the enzymatic catalysis. The measurements were performed using a Nanodrop One instrument from Thermo scientific.

3.2.6 Fluorescence spectroscopy

Fluorescence is an optical phenomenon where a molecule (fluorophore) absorbs light and then emits this light at longer wavelengths.

In fluorescence spectroscopy the sample is excited by a beam of light that is directed through a monochromator and the emission intensity is scanned over the wavelength range of interest. Fluorescence spectroscopy can be used to identify and quantify specific compounds in a sample. It is a simple method with high sensitivity and specificity.

To quantify each type of enzyme that was co-immobilized in MCF (papers III and IV), the enzymes were labeled with the Cyanine dyes: Sulfo-Cyanine3 NHS ester (Cy3) used for FateDH, Sulfo-Cyanine5 NHS ester (Cy5) for FaldDH and Sulfo-Cyanine7 NHS ester (Cy7) for ADH (Figure 22). These dyes were chosen since they have well separated absorption spectra, with absorption maxima at 550 nm for Cy3, at 650 nm for Cy5 and at 750 nm for Cy7. The quantification was also determined indirectly by measuring the absorption of protein-attached Cy3-FateDH, Cy5-FaldDH and Cy7-ADH in the supernatant after the immobilization.

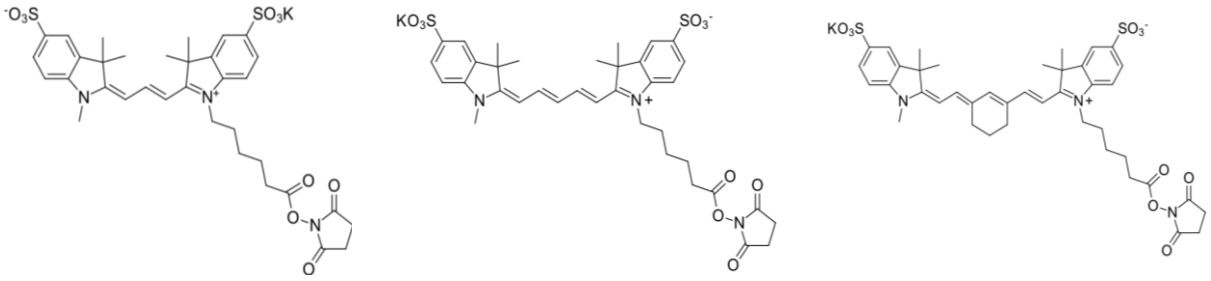

Figure 22. Molecular structure of Cy3 (Sulfo-Cyanine3 NHS ester), Cy5 (Sulfo-Cyanine5 NHS ester) and Cy7 (Sulfo-Cyanine7 NHS ester).

3.2.7 Fluorescence resonance energy transfer

Fluorescence resonance energy transfer (FRET) is an electromagnetic phenomenon where energy is transferred non-radioactively via long range dipole-dipole interaction from a donor molecule to an acceptor molecule [103]. The donor fluorophore absorbs energy which is transferred to the acceptor molecule without conversion to thermal energy or loss due to any molecular collision. For FRET to occur it is necessary that the emission spectrum of the donor overlaps with the absorption spectrum of the acceptor; also the two molecules need to be in close proximity (usually 1-10 nm) and the dipole orientations need to be parallel [103-105].

The fraction of the energy that is absorbed by the donor and transferred to the acceptor is the called efficiency of FRET (E) and can be calculated by the equation (18) where "k_T" is the rate of the energy transfer, and "τ_D" is the decay time of the donor in the absence of the acceptor [103-105].

$$E = k_T / (\tau_D^{-1} + k_T) \qquad (18)$$

The value of *"E"* can be obtained experimentally with time-resolved fluorescence measurements, and calculate "E" using the ratio of the life-time of the donor in absence (τ_D) or presence (τ_{DA}) of the acceptor (equation 19) [103-105].

$$E = 1 - (\tau_{DA} / \tau_D) \qquad (19)$$

Once *"E"* is known, it is possible to estimate the distance between the two fluorophore molecules due to the fact that "E" is inversely proportional to the sixth power of the distance (r) between them as shown in equation 20, where "R_0" is the Förster distance when the energy transfer has a 50 % efficiency. The value of "*Ro*" depends on the specific pair of fluorophores [103-105].

$$E = R_0^6 / (R_0^6 + r^6) \qquad (20)$$

The value of *"R_0"* can be calculated according to equation 21 where "κ" is the orientation factor that describes the relative orientation of the transition dipoles of donor and acceptor, "Φ_D" is the fluorescent quantum yield of the donor in the absence of the acceptor, "*J"* is the spectral overlap integral between donor emission and the acceptor absorption spectra and n is the effective refractive index [103-105].

$$R_0 = 0.211(\kappa^2 n^{-4} \Phi_D J(\lambda))^{1/6} \qquad (21)$$

In Figure 23, an example of the correlation between the FRET efficiency and the distance between fluorophores is shown.

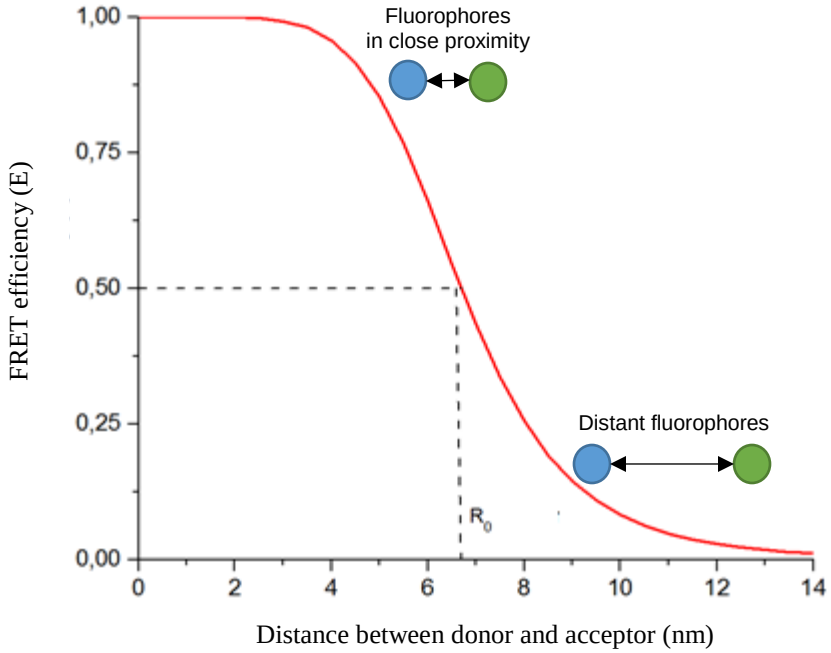

Figure 23. FRET efficiency as a function of the fluorophores distance.

In order to choose the optimum fluorophore probes for FRET analysis some considerations have to be taken into account. First, the lifetime of the fluorophore must be comparable to the timescale of the experiment; secondly, the emission spectrum of the donor dye must overlap to a large extent with the absorption spectrum of the acceptor [104]. Cyanine dyes as Sulfo-Cyanine3 NHS ester (Cy3), Sulfo-Cyanine5 NHS ester (Cy5) (Figure 22) can be used for this purpose, with Cy3/Cy5 acting as a FRET-pair which R_0 is 6.7 nm. These dyes are also considered good for studying enzyme immobilization in mesoporous silica since they can be covalently bound to the enzyme, they are negatively charged, preventing interactions with the silica wall and are photostable [106].

3.2.8 Gas chromatography

Gas chromatography is an analytical technique used to separate and analyse substances that can be vaporized without decomposition [107]. In order to separate the analytes, the samples are vaporized and carried by an inert gas (mobile phase) through the stationary phase which consists of a microscopic layer of liquid or polymer on an inert solid support, called column (Figure 24) [107]. Depending on its interaction with the column, each analyte will elute at a different time, known as retention time [107].

In the end of the column there is a detector used to provide a quantitative measurement of the compounds present in the sample [107, 108]. Among many different detectors, flame ionization detectors (FID) is the most generally used [108]. It has the advantage of being unaffected by water, flow rate, and non-combustible gases. It presents high sensitivity and low noise. In FID the sample passes through a hydrogen-air flame column creating ions due to the combustion or chemical decomposition of the compounds [108].

In this thesis the amount of methanol produced in the cascade reaction was determined using a Thermo Scientific Trace 1300 gas chromatograph with a polar column (ZB-WAX column 30 × 0.25 ×0.25) and FID detector. The carrier gas was hydrogen with a flow rate of 1.2 ml·min^{-1}. The injector temperature was 220 ºC with a column temperature of 55 ºC for 3 min, then from 55 ºC to 220 ºC at 20 ºC·min^{-1}.

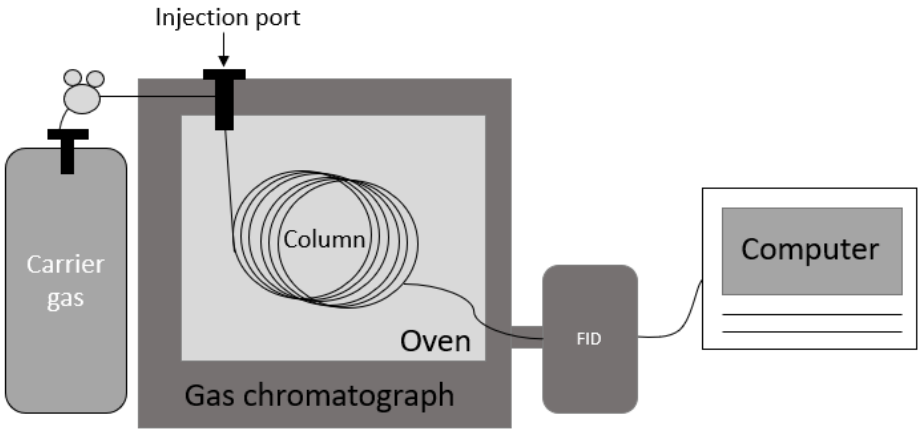

Figure 24. Schematic illustration of GC-FID.

4. Results and discussion

4.1 Immobilization of FateDH, FaldDH and ADH individually in MCF

4.1.1 Characterization of siliceous mesostructured cellular foams

Two siliceous mesostructured cellular foams, here called MCF1 and MCF2, were synthesized for the immobilization of FateDH, FaldDH and ADH separately. In the SEM images in Figure 25 it is possible to visualize the two different morphologies of MCF1 and MCF2. MCF1 is formed by the agglomeration of large spheres which sizes varies between 1 to 7 µm, whereas MCF2 is formed by smaller particles of about 1-2 µm with morphology tending towards rods.

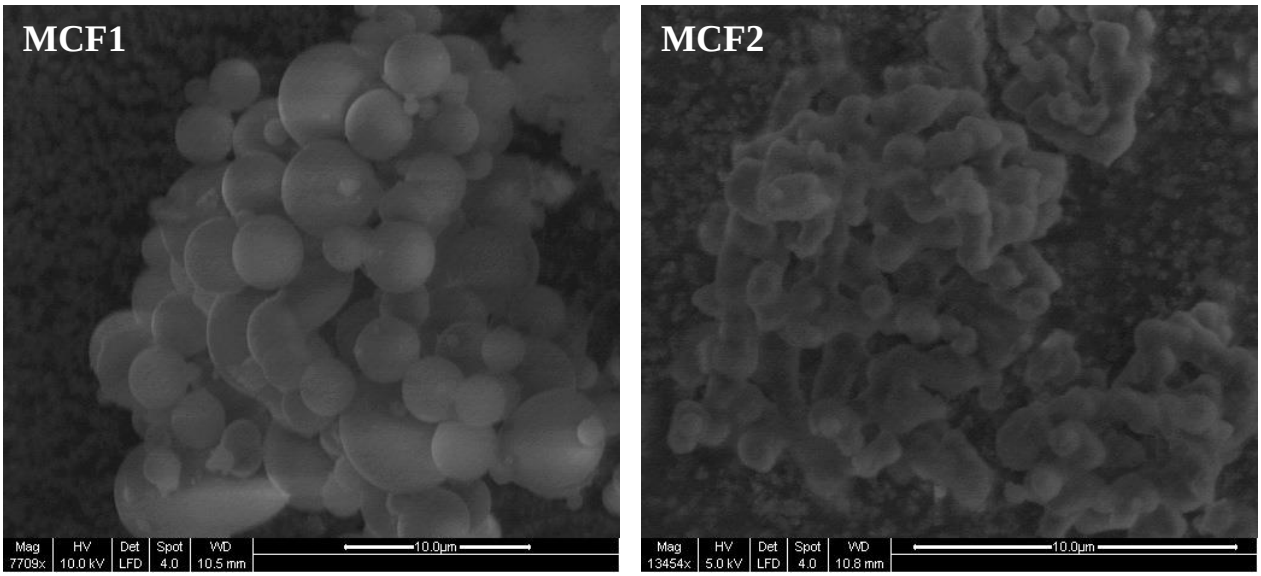

Figure 25. Representative SEM image of MCF1 and MCF 2.

The materials were also characterized by nitrogen sorption analysis (Figure 26) and their physical properties are shown in Table 4. Due to the lower amounts of TMB used in the synthesis of MCF1, this material has narrower pore and window sizes and lower surface area and pore volume than MCF2. In general, the incorporation of the functional groups led to slightly smaller window and pore diameter in comparison to the non-functionalized MCF1 and MCF2. It is also possible to notice in Table 4, a more significant decrease in the surface area and pore volumes after the surface functionalization.

The window and pore sizes of MCF1, are in principal large enough to accommodate the three enzymes, considering that FateDH has a hydrodynamic radius of 3.5 nm [109], FaldDH a molecular size of 8.6 nm x 8.6 nm x 19 nm [41] and ADH has a hydrodynamic radius of 4.55 nm [110]. MCF2 with larger window and pore sizes were synthesized aiming to evaluate the effect of the physical properties of the material in the activity of FaldDH, which is the biggest enzyme in the system.

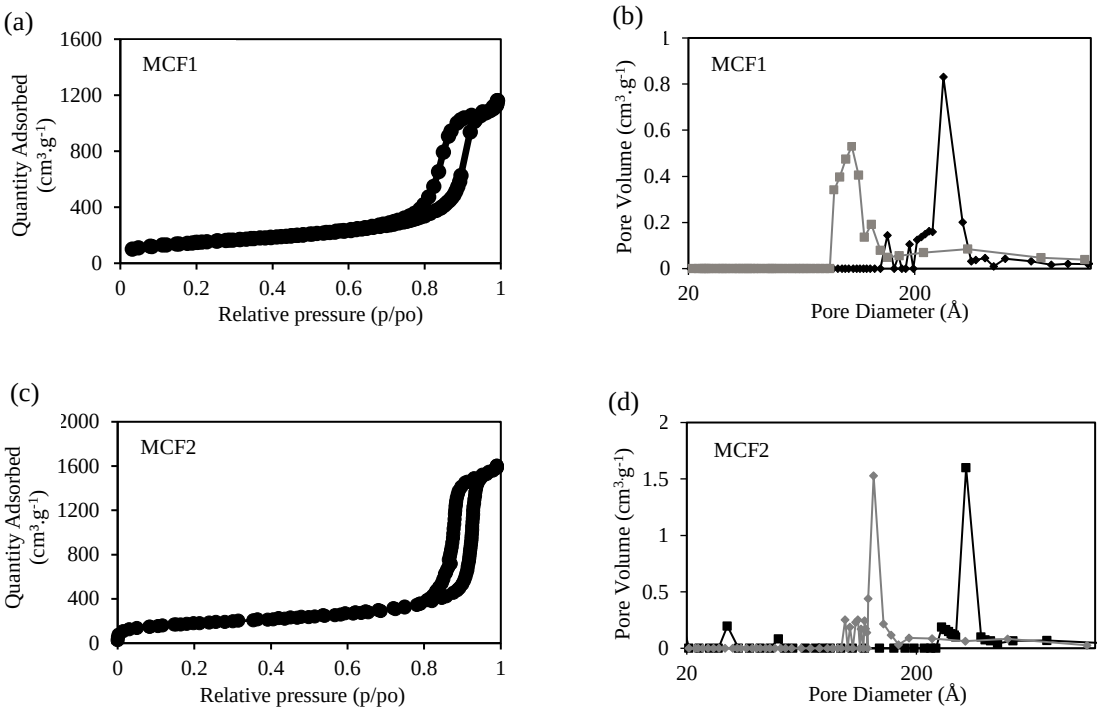

Figure 26. Nitrogen sorption measurements. (a) and (c) nitrogen adsorption-desorption isotherms for MCF1 and MCF2, respectively; (b) and (d) pore size distribution (black line) and window size distribution (grey line).

Table 4. Physical properties of MCFs.

Sample	Average window size (nm)	Average pore size (nm)	Specific surface area ($m^2 \cdot g^{-1}$)	Specific pore volume ($cm^3 \cdot g^{-1}$)
MCF1	10.5	26.8	541	1.81
MCF1-CM	10.5	26.3	494	1.68
MCF1-MP	10.6	25.4	453	1.69
MCF1-OC	9.91	25.6	443	1.62
MCF1-AP	10.5	25.9	313	1.29
MCF2	13.0	32.9	648	2.45
MCF2-CM	12.9	32.6	564	2.22
MCF2-MP	13.0	32.9	573	2.36
MCF2-OC	12.9	32.5	580	2.34

The quantification of the surface functionalization was done by TGA (Figure 27). Considering the weight losses, it was possible to calculate the surface loadings and the surface densities (Table 5). Given that each organosilane reacts with 2 silanol groups and that the silanol surface density of amorphous silica is 4.6-5.7 $OH \cdot nm^{-2}$ [55], it can be estimated that a certain amount of the free silanol would remain free in the surface after the functionalization. The lowest surface loading and density was found for the MCF modified with octyltriethoxysilane (MCF-OC). This is most

probably due to the long carbon chains that sterically hinder the access to free silanol groups in the surface.

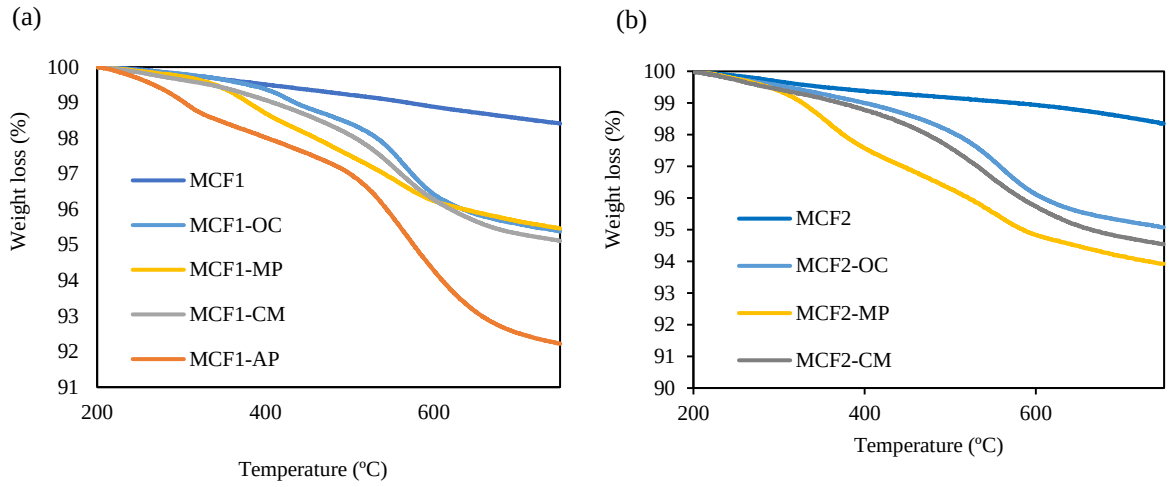

Figure 27. Thermogravimetric analysis of (a) MCF1 and functionalized MCF1 and (b) MCF2 and functionalized MCF2.

Table 5. Properties of the functionalized MCFs calculated from TGA analysis.

Sample	Weight loss (%)	Surface loading (Ns) (mmol·g^{-1})	Surface density (D) (ligand·nm^{-2})	Remaining Si-OH (#·nm^{-2})
MCF1-CM	3.2	0.6	0.7	3.8
MCF1-MP	2.8	0.5	0.5	4.2
MCF1-OC	2.9	0.3	0.3	4.6
MCF1-AP	5.9	1.0	1.1	3.0
MCF2-CM	3.8	0.8	0.7	3.8
MCF2-MP	4.4	0.8	0.7	3.8
MCF2-OC	3.3	0.3	0.3	4.6

4.1.2 Protein loading

FateDH, FaldDH and ADH were immobilized in all the versions of MCF1 at pH 5.6 and 7.0. The protein loadings, *i.e.* the amount of enzyme immobilized per gram of MCF, are show in Figure 28. At pH 5.6 higher amounts of enzymes were immobilized, since at this pH the net charge of three enzymes are close to zero and therefore there are less repulsive enzyme-enzyme interactions. At pH 7.0, on the other hand, the enzymes are negatively charged which could result in electrostatic repulsion between the enzymes and silanol groups in the MCF1 surface.

The functionalization with octyl, mercaptopropyl and chloromethyl groups seemed to improve the loading capability of FateDH and FaldDH in MCF1 at both pHs. This relative increase in the protein loading at pH 7.0 is probably due to the presence of the functional groups that hindered the close contact between the enzymes and the remaining silanol groups in the surface. On the other hand, the functionalization with aminopropyl groups led to very low to almost no immobilization of the three enzymes. This was unexpected especially at pH 7.0 in which the amine groups are positively charged and could interact with the negative charges in the enzyme surface by electrostatic interactions. However, probably due to these strong interactions between the enzyme and MCF1-AP, few enzymes could strongly adsorb in the pore entrance, hindering the diffusion of more enzymes in the core of the particles, resulting in very low protein loadings. Due to these results MCF2 was not functionalized with aminopropyl groups and MCF1-AP was not used in the activity tests.

In all the other materials (MCF1-OC; MCF1-MP; MCF1-CM), the maximum protein loading of the three enzymes at pH 5.6 can be considered satisfactory. For FateDH, the highest loading was observed in MCF-MP (Figure 28 (a)); for FaldDH the use of MCF-CM led to the highest loading (Figure 28(b)), whereas for ADH more enzymes were immobilized in the non-modified MCF (Figure 28(c)).

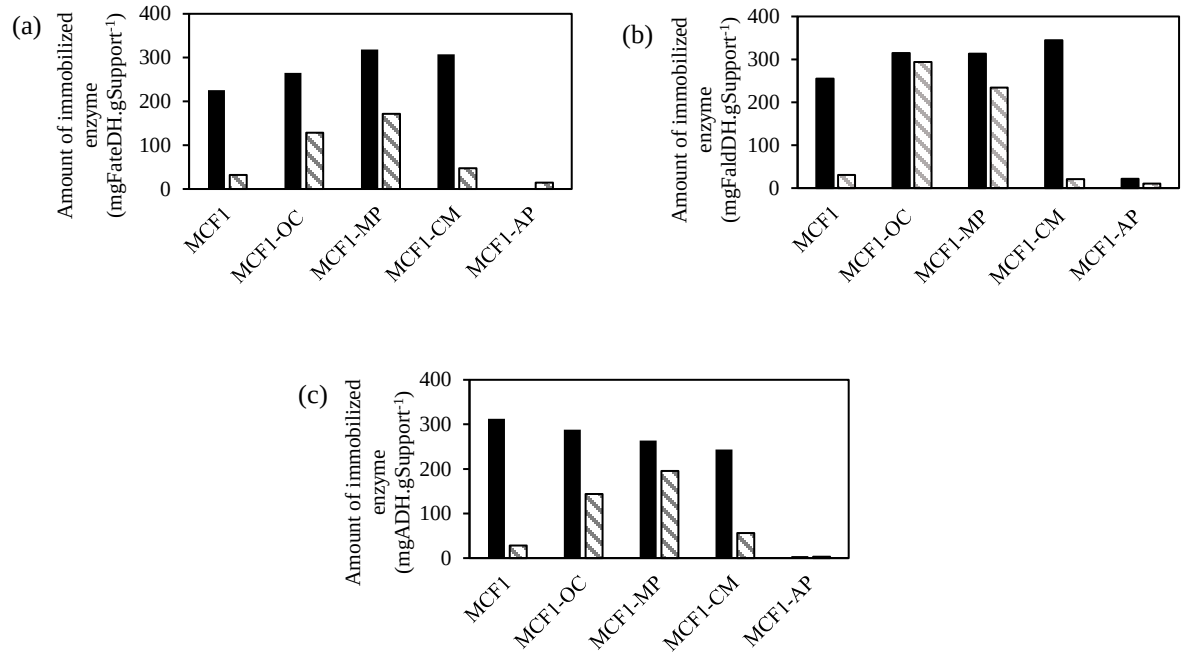

Figure 28. Immobilization of (a) FateDH, (b) FaldDH and (c) ADH in all versions of MCF1 at pH 5.6 (■) and pH 7.0 (▧).

The pore fillings were estimated for the enzyme immobilizations at pH 5.6. For these calculations it was considered that all the enzymes were immobilized inside of the pores. In Figure 29 is shown that for FateDH and ADH the enzymes occupied in average 25 % of the total volume available in MCF1s. For FaldDH, which is a larger enzyme, more than 50 % of the pores in MCF1 were filled by the enzymes.

FaldDH was also immobilized in all the versions of the MCF2 at pH 5.6. As it can be seen in Figure 30, the larger windows and pores in the MCF2 led to an increase in the maximum amount of FaldDH that could be immobilized in this material in comparison with MCF1. The loading capability of MCF2 was about 780 $mg_{FaldDH} \cdot g_{MCF2}^{-1}$, and even higher in the functionalized materials. The pore fillings calculated for these samples were estimated to be higher than 100 % of the pore volume of MCF2s. This is a clear evidence that FaldDH adsorbs not only inside the pores but also on the outer surface of the materials. Those enzymes immobilized on the outer surface could, in principal, desorb more easily than the ones immobilized inside the pores and also the "protection" and stabilization provided by the microenvironment inside of the cavities would not be achieved.

The higher enzyme loading capability in MCF2 than MCF1 can also be related to the particle size. As shown in Figure 25, MCF1 is formed by larger particles than MCF2. In smaller particles as in MCF2 the enzymes can diffuse easier through the core of the particle leading to higher protein loadings. Moreover, small particles have higher external surface area allowing more enzymes to become immobilized on its outer surface. It is important to mention that FaldDH was used as received from the supplier without any purification, so it is unknown if any impurity presence in the enzyme sample would somehow affect the immobilization.

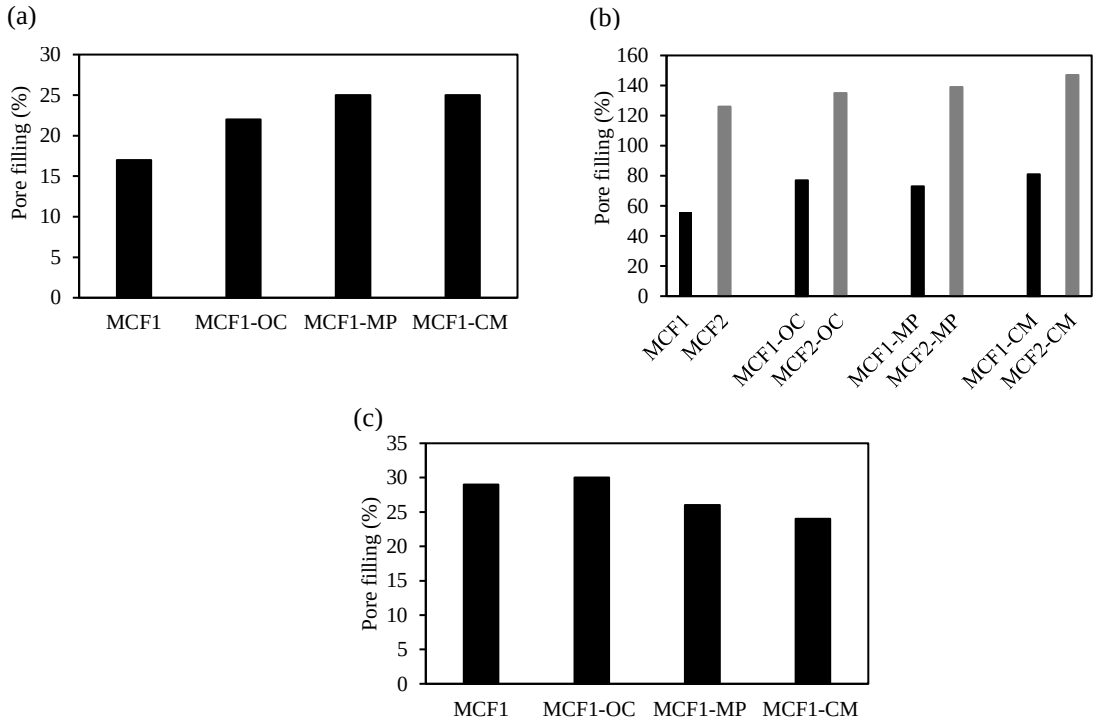

Figure 29. Percentages of the pore volume occupied by (a) FateDH, (b) FaldDH and (c) ADH assuming that all the enzymes are immobilized inside of the pores.

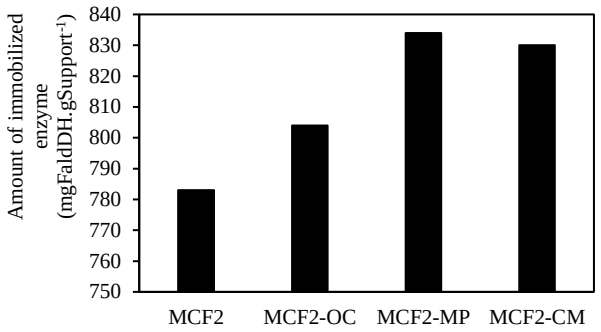

Figure 30. Immobilization of FaldDH in all versions of MCF2 at pH 5.6.

4.2 Catalytic activity of the individual enzymes

To study the catalytic activity of each enzyme, they were immobilized separately in all the versions of MCF1 (except MCF1-AP) at pH 5.6. FaldDH was also immobilized in MCF2s. The protein loadings (PLD) in the materials were lower than the maximum possible, to avoid mass transport limitations, pore blocking and loss in activity due to restrictions in the conformational changes of the enzyme during the reaction. For FateDH and FaldDH PLD of150 $mg \cdot g^{-1}$ was used whereas for ADH the loading was 130 $mg \cdot g^{-1}$.

4.2.1 Catalytic activity of FateDH

The catalytic activity of FateDH was not possible to be detected for the free or immobilized enzyme. No improvement in the reaction was observed by increasing substrate and NADH concentration or performing the reaction under 5 bars pressure. Since this enzyme is very effective for the reverse reaction, the conversion of formate $\rightarrow CO_2$ (see $\Delta_r G'^{o}$ in Table 2), it is possible that, even though, formic acid was formed, it was rapidly consumed by the enzyme. Therefore, to study the activity of this enzyme, one possibility is to add FaldDH in the reaction system, so FaldDH would consume the formate, avoiding the back reaction of FateDH.

4.2.2 Catalytic activity of FaldDH

The catalytic activity of FaldDH was possible to be measured only when high concentrations of NADH (100 mM) was used and under pressure of 5 bars. Its specific activity was found to be

0.83 mmol·gFaldDH^{-1}·min^{-1} under those conditions. In lower concentrations of NADH and milder conditions, the production of formaldehyde was too low and not detectable.

However, once immobilized in all versions of MCF1, FaldDH lost its activity and no formaldehyde could be measured. To investigate the reason for the loss in activity some conditions used for the immobilization, as pH and temperature, were modified. Using pH 7.0 instead of 5.6 or decreasing the immobilization temperature to 7 ºC, did not result in any improvement. Then, the protein loading was reduced to 50 mg·g^{-1}, to investigate if steric hindrance was causing the loss in activity, but again no activity could be measured. The loss in the activity of the immobilized FaldDH could then be related to the physical and/or chemical properties of MCF1. Therefore, FaldDH was also immobilized in MCF2 with and without surface functionalization. Upon immobilization in all the versions of MCF2, it was observed that the activity of FaldDH was retained or even increased (Figure 31). These results suggest that the physical properties of MCF1 were not suitable for the immobilization of FaldDH. Inside the smaller pores of MCF1 the flexibility of this enzyme was probably restricted, whereas, inside the larger pores in MCF2 the enzyme likely had higher mobility and could undergo conformational changes required for the catalysis.

The highest activity of FaldDH was observed when this enzyme was immobilized in MCF2-MP (Figure 31). It suggests that the thiol groups and the short carbon chain present in the MCF surface could be interacting with some amino acid residues in the enzymes, stabilizing the enzyme and/or orienting the active site in an optimum position.

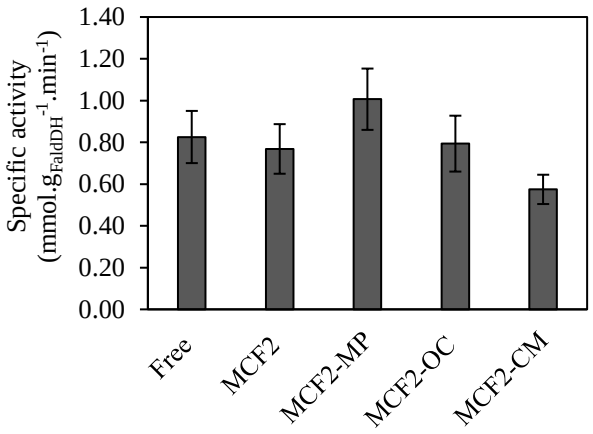

Figure 31. Specific activity of FaldDH free and immobilized in all versions of MCF2. Reaction conditions: 50 mM HCOONa; 100 mM NADH; 100 mM phosphate buffer pH 6.5; 37ºC and 5 bars pressure under CO_2 atmosphere.

4.2.2.1 Leakage of FaldDH

The adsorption stabilities of FaldDH in all the versions of MCF2 were evaluated by measuring leakage of the enzymes from each material under the reaction conditions. Very low leakage could be observed (Table 6) from all the materials, indicating that the enzyme-support interactions are rather strong. A factor that might have contributed to the low leakage is the cage-like structure of the pores. The narrower entrances (windows) probably helped to hinder the enzymes to leak out from the large pores.

The lowest leakage was observed when FaldDH was immobilized in MCF-MP. It demonstrates that the interactions between the mercaptopropyl groups and enzymes do not only increase the specific activity of the enzyme but also result in high adsorption stability.

Table 6. Percentage of FaldDH that leaked out during the reaction.

Support material	Leakage (%)
MCF2	4.5
MCF2-MP	1.8
MCF2-OC	3.4
MCF2-CM	5.1

4.2.3 Catalytic activity of ADH

Among the three enzymatic reactions required for conversion of CO_2 to methanol, the conversion of formaldehyde to methanol catalysed by ADH is the only one which is thermodynamically favourable (Table 2). Therefore, it was possible to measure its catalytic activity using low concentrations of NADH and under air (Figure 32). After immobilization in MCF1 the catalytic activity of the enzyme was retained. In MCF1-CM and MCF-MP, the specific activity of ADH decreased, whereas in MCF-OC a small increase in the activity was observed. These results suggest that the introduction of hydrophobic motifs in the MCF-OC, can be beneficial for the activity of this enzyme. Some studies have suggested that the increased activity of enzymes inside of hydrophobic cavities might be related to gain in enzyme stability (the folded state is more stable due to entropic effects), and/or favourable conformational changes in the enzymes, *e.g.* the hydrophobic interactions can lead proteins to lose their α-helix and gain β-sheet structure [80, 81].

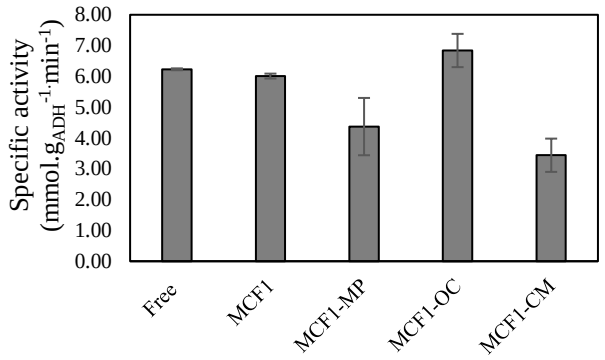

Figure 32. Specific activity of ADH for the conversion of formaldehyde to methanol. Reaction conditions: 3 mM HCHO; 1.5 mM NADH; 100 mM phosphate buffer at pH 6.5 and 25 ºC under air.

The specific activity of ADH was also evaluated under the conditions considered optimum of the enzymatic cascade reactions to convert CO_2 to methanol (NADH 100 mM, 5 bars pressure of CO_2 atmosphere). Figure 33 shows that the activity of ADH decreased significantly when such conditions were applied. To investigate the cause of the loss in activity, the influence of CO_2 atmosphere, pressure and substrate concentration were analysed separately. The following three additional experiments were thus made: 1) Cascade reaction condition under N_2 instead of CO_2 atmosphere; 2) Reaction under the normal conditions but using 5 bar pressure; 3) Cascade reaction condition with increased concentration of formaldehyde. The results obtained are shown in Figure 34.

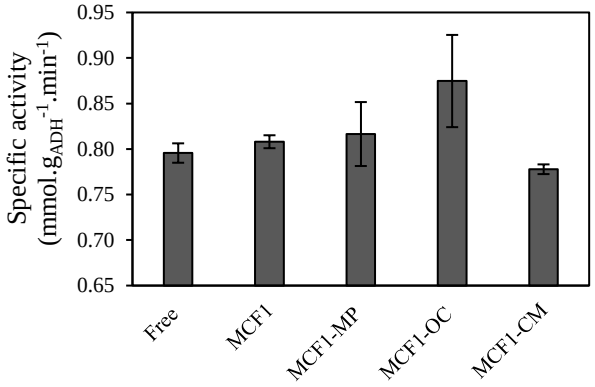

Figure 33. Specific activity of ADH for the conversion of formaldehyde to methanol under the cascade reaction conditions (50 mM HCHO; 100 mM NADH; 100mM phosphate buffer at pH 6.5; 25 ºC and 5 bars pressure under CO_2 atmosphere).

.

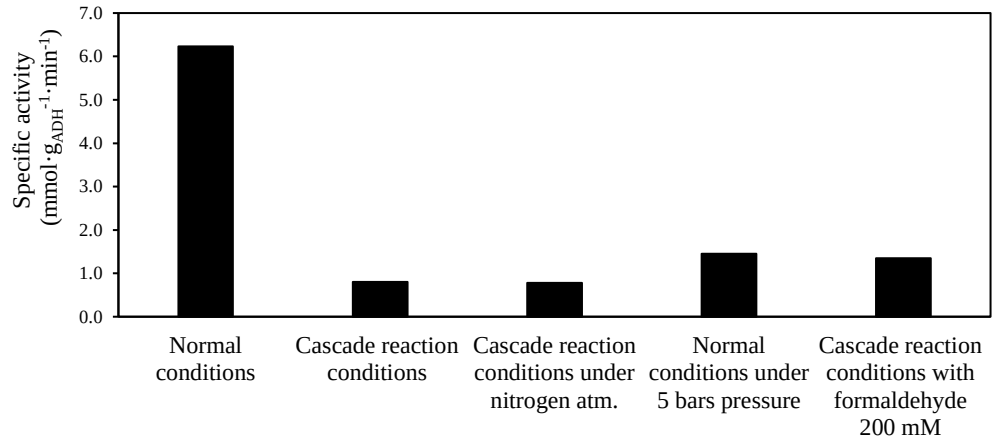

Figure 34. Comparison of the specific activity of free ADH for the conversion of formaldehyde to methanol under different conditions. (Normal conditions: 3 mM HCHO; 1.5 mM NADH; 100mM phosphate buffer at pH 6.5 and 25 ºC under air. Cascade reaction conditions: 50 mM HCHO; 100 mM NADH; 100mM phosphate buffer at pH 6.5; 25 ºC and 5 bars pressure under CO_2 atmosphere).

Under CO_2 atmosphere the pH of the system reduces from 6.5 to 5.8, which could affect the enzyme activity. However, the experiment (1) using N_2 instead of CO_2, did not result in higher conversion rates. In the experiment (2), a drastic reduction in the activity was observed when pressure was applied in the reactions using the normal conditions. This can be due to the fact that some oligomeric enzymes as ADH can dissociate in monomers under pressure reducing the enzyme activity. In experiment (3) by increasing the concentration of formaldehyde to 200 mM the activity of the ADH increased about 70 % in comparison with the activity obtained under the cascade reaction condition.

From these results it was demonstrated that ADH activity is affected by substrate concentration and pressure. Therefore, the cascade reaction conditions previously used in the literature for the conversion of CO_2 to methanol are not optimum for this enzyme.

4.3 Catalytic activity of co-immobilized FateDH and FaldDH

FateDH is not an efficient catalyst for the conversion of CO_2 since the reverse reaction is more favourable thermodynamically and kinetically. To drive the reaction towards the reduction pathway, one possibility is to add FaldDH to the reaction system, in a way that it would consume the formate as soon as it is produced by FateDH avoiding the back reaction (oxidation of formate).

This cascade reaction system of FateDH and FaldDH was evaluated for the enzymes free in solution and co-immobilized. Considering that the activity of FaldDH increased when it was immobilized in MCF2-MP, MCF3 with similar pore size as MCF2 was synthesized and its surface

was modified with mercaptopropyl groups. MCF3 and MCF3-MP were used to co-immobilize the enzymes. Figure 35 shows the pore size distribution from nitrogen sorption measurements for MCF3. Its physical properties are in Table 7.

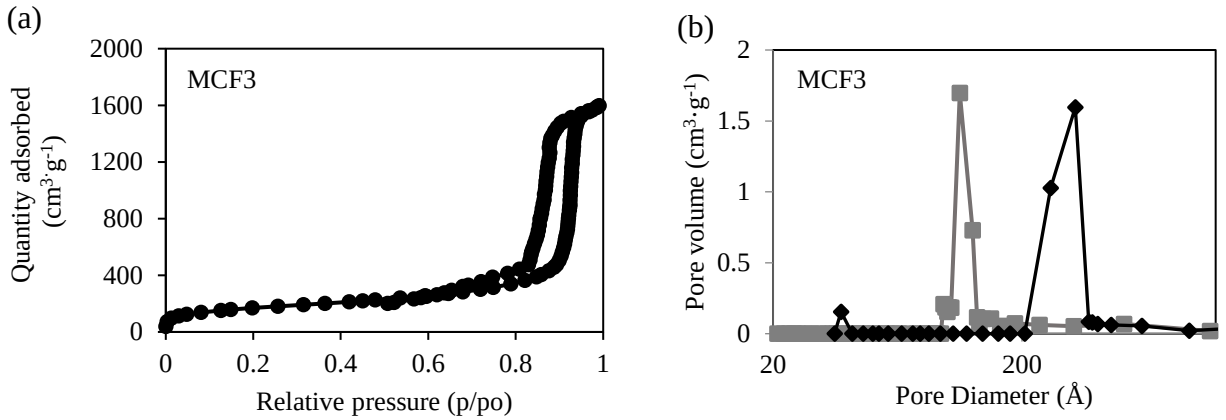

Figure 35. Nitrogen sorption measurements for MCF3. (a) Nitrogen adsorption-desorption isotherms and (b) pore size distribution (black line) and window size distribution (grey line).

Table 7. Physical properties of MCF3 and MCF3-MP.

Sample	Average window size (nm)	Average pore size (nm)	Specific surface area ($m^2 \cdot g^{-1}$)	Specific pore volume ($cm^3 \cdot g^{-1}$)
MCF3	11.3	32.8	612	2.45
MCF3-MP	11.3	32.9	527	2.27

Initially two methods of immobilization were tested, simultaneous immobilization and sequential immobilization. When the two enzymes were immobilized simultaneously no formaldehyde formation could be measured, whereas when the two enzymes were immobilized in a consecutive way (*i.e.* first formate was immobilized with the support material and then FaldDH was immobilized) it was possible to measure the production of formaldehyde and determine the activity of the cascade reaction system in all the conditions tested (Figure 36). The quantification of the amount of enzyme immobilized in each method was possible by using labelled enzymes with the dyes Cy3 and Cy5 for FateDH and FaldDH, respectively. These dyes have a well-separated absorption spectra, allowing the individual quantification of each enzyme immobilization degree By measuring UV-Vis absorbance at 280 nm of the total enzyme (without labelling) remaining in the supernatant it was not possible to quantify the concentration of FateDH that became

immobilized since the concentration was too low to be measured in the nanodrop instrument and not possible to be differentiated from the FaldDH. The results using labelled enzymes showed that, using simultaneous co-immobilization only 15% of the FateDH became immobilized whereas the consecutive immobilization led to the immobilization of more than 90% of the enzyme (Table 8). These results suggest that FaldDH has higher affinity to the materials surface than FateDH and therefore, immobilizes preferentially. Then, since FaldDH is a bigger enzyme than FateDH, it could become immobilized in the pore entrances hindering the immobilization of FateDH.

Table 8. Degree of immobilization of each enzyme after co-immobilization in MCF using the concentration ratio FateDH: FaldDH = 1:15.

Method	DOI Cy3-FateDH[a] (%)	DOI Cy5-FaldDH[a] (%)	Total amount of immobilized enzyme with labelling (%)[b]	Total amount of immobilized enzyme without labelling (%)[c]
Simultaneous	15	95	90	94
Sequential	95	95	95	95

[a]Degree of immobilization (DOI) calculated from absorption of Cy3- and Cy5-labeled enzymes.
[b]Calculated from absorption of total enzyme in the supernatant at 280 nm using the degree of labeling and the absorption of Cy3 and Cy5, respectively at 550 and 650 nm.
[c]Calculated from absorption of total enzyme in the supernatant at 280 nm using extinction coefficient $E^{1\%} = 10.0$, since FaldDH was used with higher concentration than FateDH.

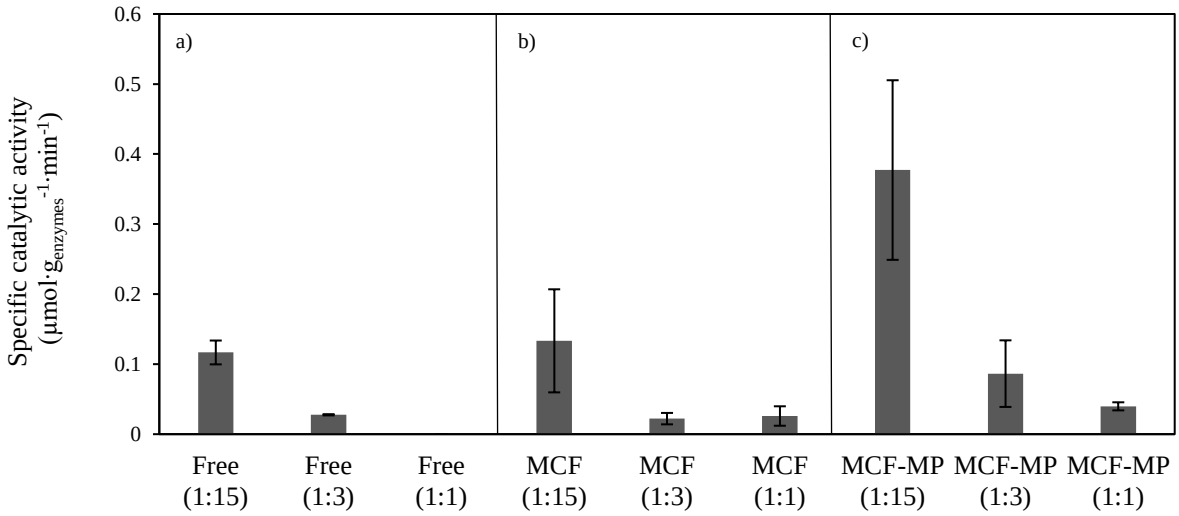

Figure 36. Specific activity of the cascade reaction using FateDH and FaldDH (a) free in solution, and co-immobilized in (b) MCF and (c) MCF-MP. The enzymes were co-immobilized using the sequential method. In parenthesis are the mass ratio of FateDH: FaldDH used in the reactions. (Reaction conditions: 200 mM $KHCO_3$; 100 mM NADH; 100 mM phosphate buffer at pH 6.5; 37 ºC and 5 bars pressure under CO_2 atmosphere).

The specific catalytic activity of the cascade reaction using the enzymes free in solution with a mass ratio of 1:15 (FateDH:FaldDH), was found to be 0.12 $\mu mol \cdot g_{enzymes}^{-1} \cdot min^{-1}$. This ratio has been reported before as optimum for this cascade reaction[18]. The co-immobilization of the enzyme (using the consecutive method) in MCF3 did not result in higher enzyme activity, whereas the immobilization in MCF3-MP increased the catalytic activity of the cascade by about 4 times. These results show that the functionalization with mercaptopropyl groups is not only beneficial for the activity of the FaldDH but also improves the cascade system. The functional groups could influence the localization of the enzymes in the material or could change the orientation of the enzymes inside the pores.

Two other enzyme mass ratios were evaluated, 1:1 and 1:3 (FateDH:FaldDH), where the concentration of FaldDH was kept constant and the concentration of FateDH was increased. However, the higher concentration of FateDH in relation to FaldDH reduced the efficiency of the cascade system with the enzymes free and immobilized in the materials.

Since the reduction of formate by FaldDH competes in the system with the oxidation of formate by FateDH, which is a thermodynamically favourable reaction (Table 2), high concentrations of FaldDH seems to be required to drive the cascade towards the reduction pathway.

4.3.1 Relation between the catalytic activities of the cascade reaction with the distance between the enzymes

Förster resonance electron transfer (FRET) analyses were performed to understand the increase in catalytic activity when the enzymes were co-immobilized in MCF3-MP in caparison with the immobilization in MCF3 or free in solution. For this, FateDH and FaldDH were labelled with the dyes Cy3 and Cy5, respectively.

It was observed, as shown in Table 9, that the efficiency of the energy transfer (*E*) between the dyes was higher when the enzymes where immobilized in MCF3-MP than in MCF, using the enzyme ratio 1:15 (Cy3-FateDH:FaldDH-Cy5). This result indicates that the dyes (enzymes) are in closer proximity when immobilized in MCF3-MP. This could potentially lead to substrate channelling improving the catalytic activity of the cascade reaction. When higher concentrations of FateDH was used, a decrease in the energy transfer (*E*) for the enzymes immobilized in MCF3 and MCF3-MP was observed (Table 9). For enzymes free in solution, no FRET was detected, which shows that the average distance between the enzymes is considerably larger than R_0 (R_0 = 6.7 nm for the Cy3/Cy5-pair) (Figure 23).

Table 9. Energy transfer efficiency of enzymes co-immobilized in MCF3 and MCF3-MP at different enzyme concentration ratios.

	MCF[a]			MCF-MP[a]		
Ratio[b]	1:15	1:3	1:1	1:15	1:3	1:1
E[c]	0.56±0.02	0.44±0.02	0.20±0.02	0.64±0.02	0.55±0.02	0.36±0.02

[a]Total protein loading 150 $mg_{enzymes} \cdot g_{support}^{-1}$.
[b]Mixing ratio Cy3-FateDH: FaldDH-Cy5.

4.4 Catalytic activity of co-immobilized FateDH, FaldDH and ADH

To study the catalytic activity of the cascade reaction to convert CO_2 to methanol, MCF4 was synthesized and functionalized with mercaptopropyl groups (MCF4-MP). MCF 4 has similar physical properties as MCF3 as shown in Figure 37 and Table 10. The incorporation of the functional groups in MCF4-MP was confirmed and quantified by TGA (Table 11).

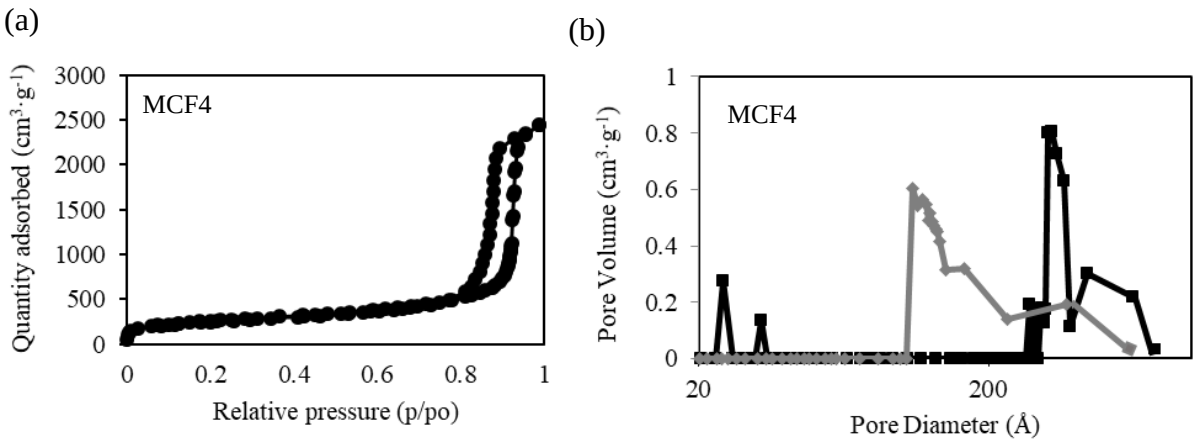

Figure 37. Nitrogen sorption measurements for MCF4. (a) Nitrogen adsorption-desorption isotherms and (b) pore size distribution (black line) and window size distribution (grey line).

Table 10. Physical properties of the MCFs analyzed by nitrogen sorption.

Sample	Average window size (nm)	Average pore size (nm)	Specific surface area ($m^2 \cdot g^{-1}$)	Specific pore volume ($cm^3 \cdot g^{-1}$)
MCF4	10.9	33.0	678	2.7
MCF4-MP	10.4	31.2	441	2.0

Table 11. Properties of the functionalized MCFs calculated from TGA analysis.

Sample	Weight loss (%)	Surface loading ($mmol \cdot g^{-1}$)	Surface density ($ligand \cdot nm^{-2}$)
MCF4-MP	4.4	0.6	0.5

The enzymes were first co-immobilized in MCF4-MP aiming for a protein loading of 150 $mg_{enzymes} \cdot g_{support}^{-1}$ (PLD150). To be able to calculate the DOI of each enzyme, they were labeled with different cyanine dyes (FateDH-Cy3; FaldDH-Cy5 and ADH-Cy7). As can be seen in Table 12, the DOIs of FateDH and FaldDH were lower than expected, considering the previous results obtained when only these two enzymes were immobilized (Table 8). Using both immobilization strategies (reaction or size order of enzyme addition) to immobilize the three enzymes, the DOIs obtained were 87% for FateDH and only 70% for FaldDH. It is likely that the protein loading used was higher than the maximum loading capability of the material when the three enzymes are present.

Table 12. DOI obtained for each enzyme in MCF-MP at aimed PLD of 150 $mg_{enzymes} \cdot g_{support}^{-1}$.

Immobilization Sequence	DOI (%) 2h			DOI (%) 4h			DOI (%) 6h		
	FateDH	FaldDH	ADH	FateDH	FaldDH	ADH	FateDH	FaldDH	ADH
Reaction order	92	-	-	89	77	-	87	70	93
Size order	92	-	-	88	-	95	87	70	93

Considering these results, the PLD was reduced to 50 $mg_{enzymes} \cdot g_{support}^{-1}$ (PLD50). The reduction in the PLD increased the DOI of all the three enzymes, as can be seen in Table 13.

Table 13. DOI obtained for each enzyme in MCF-MP at aimed PLD of 50 $mg_{enzymes} \cdot g_{support}^{-1}$.

Immobilization Sequence	DOI (%) 2h			DOI (%) 4h			DOI (%) 6h		
	FateDH	FaldDH	ADH	FateDH	FaldDH	ADH	FateDH	FaldDH	ADH
Reaction order	96	-	-	93	90	-	91	79	99
Size order	96	-	-	92	-	99	90	82	99

From the results present in Table 12 and 13 it is possible to notice reductions in the DOIs for FateDH and FaldDH during the subsequent immobilization steps. It suggests that due to the interaction between the different enzymes some of the FateDH and FaldDH desorb from the MCF-MP surface. Nevertheless, the DOIs for ADH were constantly higher than for the other two enzymes suggesting that ADH adsorbs preferentially in this material.

The enzymes co-immobilized using the two immobilizations strategies and at PLD50 and PLD150 were then used in the cascade reaction to convert CO_2 to methanol. The specific activity found for each condition was compared with the activity of the enzymes free in solution in Figure 38.

By using the free enzymes in solution, the specific catalytic activity of the cascade reaction was about 0.3 $mmol \cdot g_{enzyme}^{-1} \cdot min^{-1}$. A considerable increase in the activity was observed when the enzymes were immobilized using PLD50 (Figure 38(c)). This improvement was not as significant using PLD150 probably because at high protein loadings diffusion limitations of substrate and product may occur.

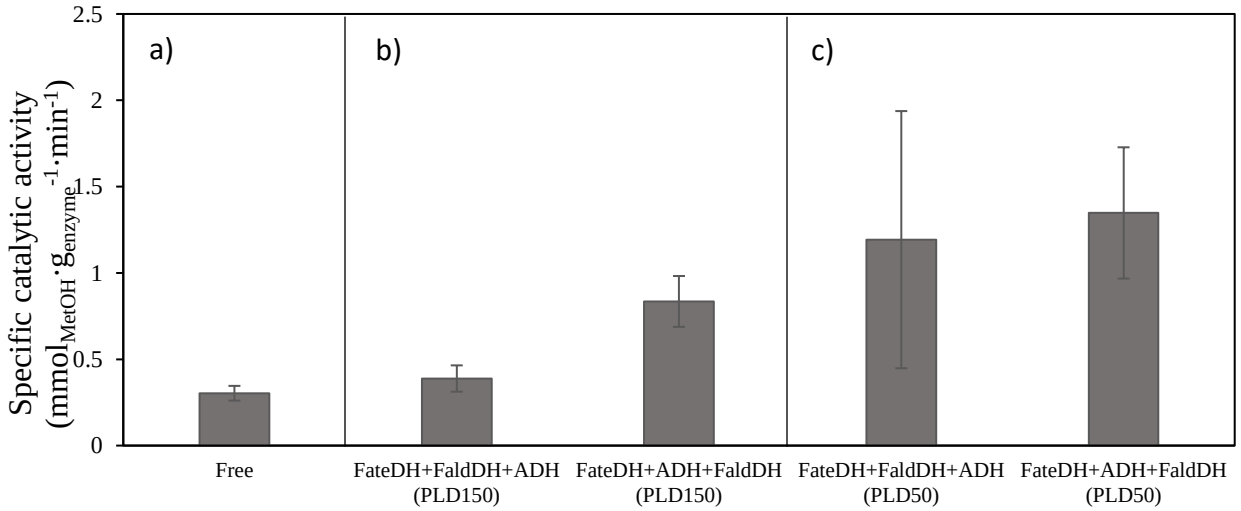

Figure 38. Specific catalytic activity of the cascade reaction using a) free enzymes; b) immobilized enzymes at aimed loading PLD150; c) immobilized enzymes at aimed loading PLD50. The specific catalytic activity calculated for immobilized enzymes were corrected considering the percentage of each enzymes that became immobilized as shown in Table 12 and 13. (Reaction conditions: 200 mM $KHCO_3$; 100 mM NADH; 100 mM phosphate buffer at pH 6.5; 37 ºC and 5 bars pressure under CO_2 atmosphere).

The highest conversion rates found in this work (1.35 $mmol_{MeOH} \cdot g_{enzyme}^{-1} \cdot min^{-1}$) with the enzymes immobilized according to their size (FateDH→ADH→FaldDH) and PLD50 is about 4.5 times higher than for the enzyme free in solution and to the best of our knowledge, this is the highest specific catalytic activity reported for the enzymatic cascade reaction under similar reaction conditions where no regeneration system for NADH was used.

The methanol productivity obtained with the immobilized enzymes are also considerably higher than the ones obtained with photocatalysis (current highest specific catalytic activity using Cu-C/TiO_2 is about 0.4 $\mu mol_{MeOH} \cdot g_{catalyst}^{1} \cdot min^{-1}$ [20]), and similar to the best results obtained using heterogeneous catalysts [11]. However, heterogeneous catalysts require high temperatures and

pressure. For example, Sahibzada [111] reported a methanol production of 1.3 $mmol_{MeOH} \cdot g_{catalyst}^{1} \cdot min^{-1}$ using Pd promoted Cu/ZnO catalysts at 250 ºC and 45 bar pressure.

There are still many challenges in practical application of technologies to convert CO_2 to methanol. Here we were able to demonstrate a simple immobilization method using an inexpensive host material to improve the catalytic efficiency of the enzymatic conversion of CO_2 to methanol. Further improvement of this biocatalytic reaction can be obtained by the addition of a regenerating system for NADH, and the application of the process in continuous flow to extract the synthesized methanol.

4.5 Spatial distribution of ADH in mesoporous silica particle

One additional study in this work was the investigation of the spatial distribution of ADH immobilized in three MPS particles, one MCF and two SBA-15 with different pore sizes.

We aimed to evaluate the ability of large enzymes as ADH to diffuse through the pores of the particles using nitrogen sorption analysis.

4.5.1 Characterization of the MPS

ADH was immobilized in three MPS. Prior to the immobilization, the materials were characterized by nitrogen sorption analysis (Table 14). Figure 39 shows the pore size distribution of the two SBA-15 synthesized. The pore and window size distribution of MCF1 were shown before in Figure 39. Its physical properties are presented again in Table 14, in order to be compared with the two SBA-15.

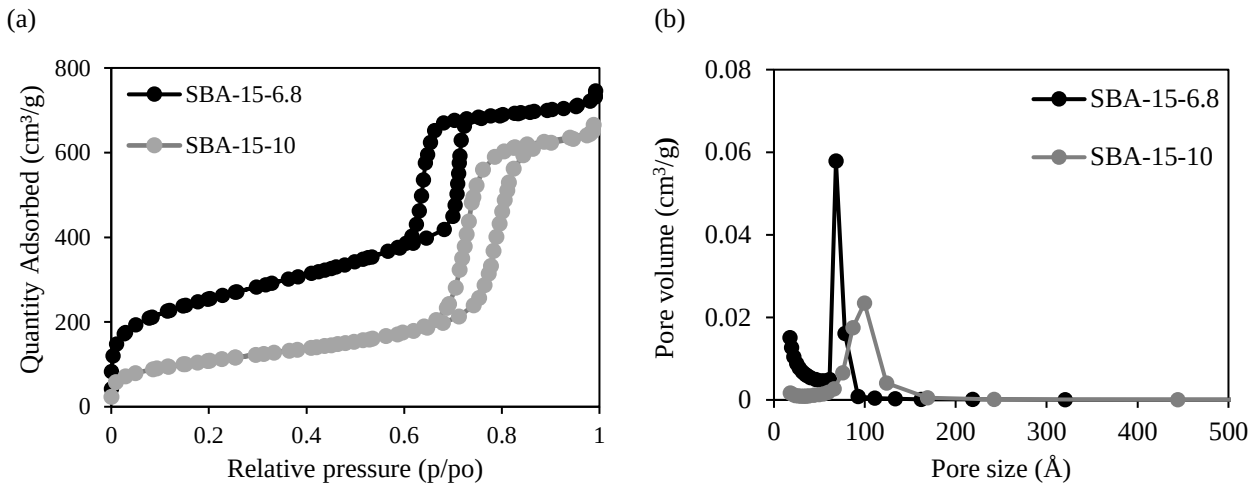

Figure 39. Nitrogen sorption measurements for SBA-15-6.8 and SBA-15-10. (a) Nitrogen isotherms and (b) pore size distribution.

The SBA-15 with average pore diameter 6.8 was called SBA-15-6.8. It has maximum pore diameter of 9 nm and, therefore, the pores are possibly too tight for ADH (hydrodynamic radius 4.55 nm) to diffuse inside. The other SBA-15 has an average pore size of 10 nm (named SBA-15-10) which are comparable with the window (pore entrance) size in MCF.

Table 14. Physical properties of the MPS as synthesized and with immobilized ADH.

Sample	Average pore size (nm)	Average window size (nm)	Surface area ($m^2 \cdot g^{-1}$)	Reduction of surface area (%)	Micropore surface area ($m^2 \cdot g^{-1}$)	Pore volume ($cm^3 \cdot g^{-1}$)	Reduction of pore volume (%)	Pore filling (%)
SBA-15-6.8	6.8	-	749	-	168	1.13	-	-
SBA-15-6.8-PB*	6.8	-	492	34	34	0.83	27	-
SBA-15-6.8-150	6.8	-	410	45	29	0.69	39	15
SBA-15-6.8-300	6.8	-	425	43	24	0.69	39	24
SBA-15-10	10.0	-	370	-	25	1.00	-	-
SBA-15-10-PB*	8.8	-	292	21	16	0.84	16	-
SBA-15-10-150	8.8	-	291	21	-	0.75	25	24
SBA-15-10-300	8.9	-	203	47	-	0.57	43	40
MCF	26.8	10.7	485	-	56	1.81	-	-
MCF-PB*	20.5	9.0	299	38	30	1.16	36	-
MCF-150	20.7	9.0	240	51	8	0.90	50	13
MCF-300	20.6	9.0	181	63	12	0.65	65	26

* Control samples with only phosphate buffer (no enzyme) during immobilization.

TEM representative images of MCF1 and the two SBA-15 in Figure 40 show the different pore morphologies of the two types of MPS. MCF1 has a strut like structure whereas SBA-15-6.8 and SBA-15-10 is formed by long cylindrical pores.

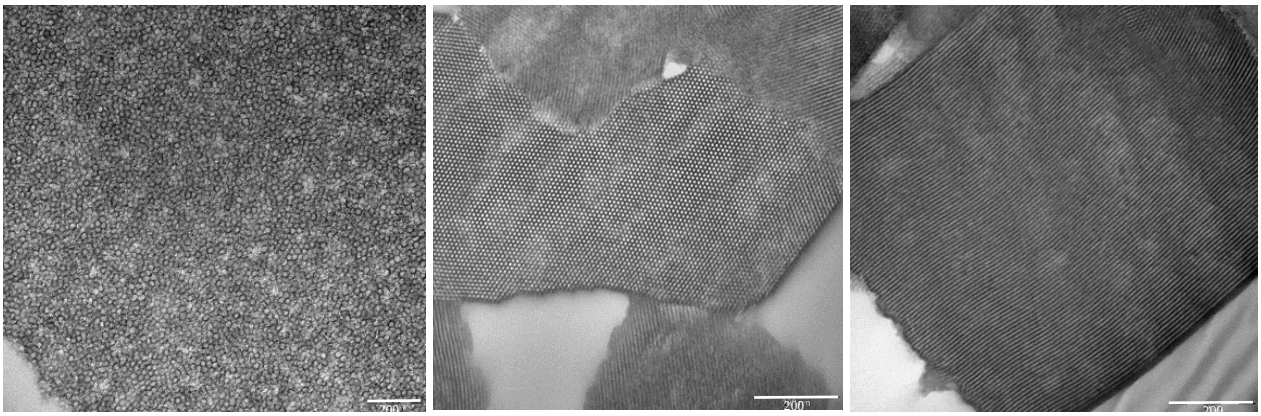

Figure 40. Representative TEM images from MCF1, SBA-15-6.8 and SBA-15-10. Scale bars are 200 nm.

4.5.2 Immobilization of ADH in MPS

The three synthesized MPS were used to immobilize the ADH. After the immobilization the samples were named as MPStype-150 or MPStype-300, according to the protein loading aimed, 150 or 300 $mg_{enzyme} \cdot g_{support}^{-1}$, respectively. Table 15 shows the protein loading obtained (PLD) and the degree of immobilization (DOI). In the MCF more than 90% of ADH became immobilized, which can be attributed to the higher porosity of this material. Comparing the immobilization in the two SBA-15s, the DOI found for SBA-15-6.8 was the lowest obtained in both conditions, whereas the amount of enzyme immobilized in SBA-15-10 was significantly larger. That was most probably due to the narrow pores in SBA-15-6.8 which hinders the diffusion of the enzymes through the pores.

Table 15. Immobilized amounts of enzymes in MPS.

Sample	Added protein ($mg_{enzyme} \cdot g_{support}^{-1}$)	PLD ($mg_{enzyme} \cdot g_{support}^{-1}$)	DOI (%)
MCF-150	300	280	93
MCF-300	150	144	96
SBA-15-10-150	300	240	80
SBA-15-10-300	150	140	93
SBA-15-6.8-150	300	160	53
SBA-15-6.8-300	150	100	67

4.5.3 Nitrogen sorption analysis of MPS after enzyme immobilization

In Table 14 is shown the physical properties of the MPS characterized by nitrogen sorption before and after the immobilization of enzymes. Considering first the effect of the enzyme immobilization on the pore size, it was observed in the control samples (only MPS in phosphate buffer (PB)) that no reduction in the mean pore size for SBA-15-6.8-PB occurred in comparison to the as-synthesized material, whereas for SBA-15-10-PB and MCF-PB, the mean pore size decreased due to the adsorption of the salt molecules in the MPS mesopores. In SBA-15-6.8-PB the reduction in the micropore surface area from 168 to 34 $m^2 \cdot g^{-1}$ suggests that the salt absorbs mainly in the micropores. In the SBA-15-10 and MCF there are considerably less micropores. For the samples where the enzymes were immobilized (aimed protein loading 150 and 300 $mg_{enzyme} \cdot g_{support}^{-1}$), it was not observed any further reduction in the mean pore size in any of the MPS, even when high loadings were obtained. In the case of the SBA-15 samples, if the enzymes are immobilized more in the pore entrance and not occupying the whole length of the pores, no reduction in the mean pore size would be expected, as observed in this study. In the MCF particle, due to its high porosity, even in the case of high loadings, it could happen that most of the pores are still unoccupied by enzymes, so the average pore size does not vary. Therefore, the effect of the enzyme immobilization in the pore size seems to not provide valuable information about the distribution of the enzymes in/on the particles.

Interestingly, the surface area and pore volume are more sensitive to the presence of the enzymes, as shown in Table 14. For SBA-15-6.8, it is possible to observe, that increasing the enzyme loading (samples SBA-15-6.8-150 and SBA-15-6.8-300, Table 14), did not result in a reduction of the surface area or pore volume, contrary to what was expected according to the theoretical calculation (using equation (8)). This result suggests that, when more enzymes are added, they become immobilized in the outer surface of the material, instead of inside of the pores. For SBA-15-10, the samples SBA-15-10-PB and SBA-15-10-150, showed the same reduction in the surface area (21%) whereas the reduction in the pore volume was 16% for SBA-15-10-PB and 24% for SBA-15-10-150. This reduction in the pore volume for SBA-15-10-150 is very similar to the one

calculated theoretically, considering that only enzymes (not salts) are adsorbed in the SBA-15-10 surface. Such observations indicate that when the enzymes are immobilized in this material, they may obstruct the pore entrance, so the salt molecules have restricted access to the interior of the pores. A further reduction in the surface area and pore volume was observed for SBA-15-10-300, suggesting that more enzymes are immobilized inside the pores.

For MCF, the higher the enzyme loading, the higher was the reduction in the surface area and the pore volume. The absorbance of salt molecules in the MCF reduced the pore volume by 36% (MCF-PB, Table 14). For MCF-150 more 14% of the pore volume was reduced (total reduction of 50%). This value agrees with the theoretical pore filling calculation, which does not take into account the presence of salt. The increase in the protein loading in MCF-300 would reduce the pore volume by 26 % according to the theoretical calculation. If it is considered that, from the total 65 % of reduction obtained, 36 % are due to the ions from the salt adsorbed in the surface, the theoretical and experimental results are again in agreement. Unlike SBA-15, MCF shows high porosity and accessibility of the pores, so enzymes and salt molecules can be adsorbed inside the pores.

The results from nitrogen sorption analysis are supported by TEM images using immunogold stanning for the visualization of the immobilized enzymes (paper V).

This study confirms MCF as a good host material for the immobilization of large enzymes as ADH. In MCF the enzymes can diffuse more efficiently through the pores and consequently higher protein loading can be obtained.

5. Conclusions

In this thesis, it was shown the advantages of using MCF for the immobilization of large enzymes and the importance of tailoring its physical and chemical properties for enzyme immobilization.

It was observed that the protein loading and the catalytic activity of the enzymes were strongly dependent on the pore size and surface functionalization of the MCF. MCF with pore size of 26.8 nm and window size of 10.5 nm could be used to immobilize FateDH and ADH, whereas FaldDH required MCF with larger pores to keep its activity. The study of the immobilization and activity of each enzyme separately in the MCFs allowed us to design the material with suitable properties to improve the cascade reactions performed by the enzymes.

MCFs with pore sizes of about 33 nm and window size of about 11 nm were first used to co-immobilize only FateDH and FaldDH. By functionalizing the MCF with mercaptopropyl groups, a significant increase in catalytic activity of the two enzymes was observed. The results from FRET measurements indicated that this improvement was likely because the two enzymes were closer to each other when immobilized in MCF-MP, and therefore the probability of substrate channelling between them increases.

The most important result was obtained with the three dehydrogenases co-immobilized for the cascade reaction to convert CO_2 to methanol. The catalytic activity of the cascade reaction of

enzymes immobilized in the MCF-MP increased about 4.5 times in comparison to the free enzymes in solution. This is the highest efficiency of the cascade reaction reported so far in the literature using systems in the same conditions (pressure, temperature and substrate/cofactor concentration) and without a NADH recycling system. This result shows that CO_2 can successfully be reduced to methanol by using a simple method of immobilization on an inexpensive material. Further improvement of the cascade reaction is expected by the addition of a regeneration system for NADH.

The work presented here gives a comprehensive understanding of enzyme immobilization in mesoporous silica in general and represents a big step towards systems using enzymatic cascade reactions to convert CO_2 to methanol.

Acknowledgment

I would like to thank the funding from the Swedish research council as part of the Linnaeus centre for Bio-inspired Supramolecular Function and Design-SUPRA.

I am also very grateful to many people that supported me during my journey to become a PhD:

First, my supervisor **Anders Palmqvist**. Thank you for giving me the opportunity to develop this research, for believing in my ideas and for all your supervision and knowledge you shared with me during these years. I remember from our first meeting when you told me how you expected my research to be and how I could develop myself as a researcher. Now I am very happy to see how everything worked so well. Once more, thanks a lot!

My co-authors **Björn Åkerman, Pegah S. Nabavi Zadeh and Gerard Masdeu.** I think I can say that we became a team and a very successful one. It was a great experience to work with you. I could learn so much with our collaboration. Thank you for your hard work.

The other two members of the SUPRA enzymes cluster: **Lisbeth Olsson** and **Cyrielle Bonzom**, for the meetings and discussions about enzyme immobilization which were very valuable for my work.

The former director of studies, now head of the division, **Hanna Härelind**, for all the support I got from you.

My examiner, **Magnus Skoglundh**, for the advices and suggestions.

The **research group** for all scientific discussions that for sure made my work better. It was really nice to be part of a group with people with so diverse background. I could learn a lot from you! Thanks also for the fun we had during the group activities.

Anne Wendel for all the help with the nitrogen sorption measurements.

Frida, Carina and Ann for all the help with administrative work.

My former supervisor, **Zareen Abbas.** I don't think I would ever start my PhD studies if you haven't given me the chance to do the master thesis in your group. I'll be always grateful for that. Thanks for being the great person that you are and for all the knowledge that I get from you in every opportunity we meet.

My lovely friends **Giulio, Saba and Ting**. My time as a PhD student wouldn't be as half as nice without you around. Thanks for cheering me up, for every talk we had, for every time we laughed together. Your friendship is priceless! I really have you as my family here in Sweden. You are awesome!

Gunnar, Sam, Mats, Anand, Johanna, Simone, Andy, Caroline, Walter, Peter, Carl-Robert and many other friends from TYK for the fun and good talks we had during fikas and afterworks.

All people from **TYK** and **KCK** for making this division a great place to work. I cannot list you all here, but you are all amazing colleagues and make this division the best place to work in Chalmers!

All my dear **friends in Gothenburg** that comes from all over the world and which names are too many to be written. Thanks for making Gothenburg an even better place to live. I am very happy that I had the chance to meet you all!

My **friends in Brazil, Gabi, Ayesha, Rodrigo, Tate, Camilinha, Paulinha, Rafael, Otavio and Filipe.** Thanks for all the efforts you make to meet us when we are in Brazil. Thanks for the barbecues and guacamoles. Thanks for the talks in our "Ludo" group. Sometimes it was so relieving to have the chance to share with you my thoughts and have the feeling that I am not alone and see that there are people in this world that can make the difference.

My **family in Brazil**. Quero agradecer imensamente minha mãe e meu pai, **Marisa e Carlos**, por toda educação que me deram, por não medirem esforços para sempre me darem o melhor e por sempre me impulsionarem a ir mais longe. Vocês sempre serão meu sustento onde quer que eu esteja. Ao meu querido irmão **Marcelo** por todos os dias que me levou para a escola, que teve muita paciência com a irmã mais nova e cujo amor sinto no olhar. A minha querida avó **Terezinha** e minha madrinha **Elvira**, essas duas mulheres guerreiras que são inspiração para mim. Obrigada por serem o exemplo que são! Aos meus tios **Ulisses, Cassia e Adalberto** por todos os dias que vocês me fortaleceram mesmo a distância! Aos meus sobrinhos, **Jéssica, Léo e Amanda**, agradeço por serem tão amorosos e sempre me encherem de alegria. Também agradeço minha sogra **Maryangela**, minhas cunhadas, **Gisela e Aline**, meus cunhados **Alexandre e Paulinho** por sempre me apoiarem e por todo acolhimento. Obrigada a todos vocês da minha família que mesmo de longe sinto sempre presente. Amo muito vocês.

The love of my life, **Adriano Gomes**! For being the best husband and daddy in the world! You always make me feel special and loved, and never let me give up my dreams! Thanks for always being there for me, for sharing your life with me and for loving me. I love you very much!

The most important person in my life, my little **Daniel**, who arrived in the middle of this journey. Thanks, for being such a nice and patient boy. Even in the days that I was more tired and stressed your smile made my heart melt and the happiness of having you in my life is impossible to describe in words.

References

1. Ganesh, I., *Conversion of carbon dioxide into methanol - a potential liquid fuel: Fundamental challenges and opportunities (a review).* Renewable & Sustainable Energy Reviews, 2014. **31**: p. 221-257.
2. Al-Ghussain, L., *Global warming: review on driving forces and mitigation.* Environmental Progress & Sustainable Energy, 2019. **38**(1): p. 13-21.
3. Qin, Z., Q. Zhuang, and X. Zhu, *Carbon and nitrogen dynamics in bioenergy ecosystems: 2. Potential greenhouse gas emissions and global warming intensity in the conterminous United States.* Global Change Biology Bioenergy, 2015. **7**(1): p. 25-39.
4. Dibenedetto, A., A. Angelini, and P. Stufano, *Use of carbon dioxide as feedstock for chemicals and fuels: homogeneous and heterogeneous catalysis.* Journal of Chemical Technology and Biotechnology, 2014. **89**(3): p. 334-353.
5. Sun, Q., et al., *Green and Efficient Conversion of CO2 to Methanol by Biomimetic Coimmobilization of Three Dehydrogenases in Protamine-Templated Titania.* Industrial & Engineering Chemistry Research, 2009. **48**(9): p. 4210-4215.
6. Amao, Y., *Photoredox systems with biocatalysts for CO2 utilization.* Sustainable Energy & Fuels, 2018. **2**(9): p. 1928-1950.
7. Allen, M.R. and T.F. Stocker, *Impact of delay in reducing carbon dioxide emissions.* Nature Climate Change, 2014. **4**(1): p. 23-26.
8. Masuda, Y., et al., *Enhancement of activity and stability of the formaldehyde dehydrogenase by immobilizing onto phenyl-functionalized mesoporous silica.* Colloids and Surfaces B: Biointerfaces, 2013. **101**: p. 26-33.
9. Aresta, M., A. Dibenedetto, and A. Angelini, *Catalysis for the Valorization of Exhaust Carbon: from CO2 to Chemicals, Materials, and Fuels. Technological Use of CO2.* Chemical Reviews, 2014. **114**(3): p. 1709-1742.
10. Aresta, M. and A. Dibenedetto, *Utilisation of CO2 as a chemical feedstock: opportunities and challenges.* Dalton Transactions, 2007(28): p. 2975-2992.
11. Sun, Y., et al., *A Critical Perspective on CO2 Conversions into Chemicals and Fuels.* Journal of Nanoscience and Nanotechnology, 2019. **19**(6): p. 3097-3109.
12. Long, N.V.D., et al., *Recent Progress and Novel Applications in Enzymatic Conversion of Carbon Dioxide.* Energies, 2017. **10**(4).
13. Olah, G.A., *Towards Oil Independence Through Renewable Methanol Chemistry.* Angewandte Chemie-International Edition, 2013. **52**(1): p. 104-107.
14. Lais, A., et al., *Experimental parameters affecting the photocatalytic reduction performance of CO2 to methanol: A review.* International Journal of Energy Research, 2018. **42**(6): p. 2031-2049.
15. Aresta, M., A. Dibenedetto, and A. Angelini, *Converting "Exhaust" Carbon into "Working" Carbon*, in *Co2 Chemistry*, M. Aresta and R.V. Eldik, Editors. 2014. p. 259-288.
16. Baskaya, F.S., et al., *Thermodynamic Feasibility of Enzymatic Reduction of Carbon Dioxide to Methanol.* Applied Biochemistry and Biotechnology, 2010. **162**(2): p. 391-398.
17. Xu, S.W., et al., *Efficient conversion of CO2 to methanol catalyzed by three dehydrogenases co-encapsulated in an alginate-silica (ALG-SiO2) hybrid gel.* Industrial & Engineering Chemistry Research, 2006. **45**(13): p. 4567-4573.
18. Cazelles, R., et al., *Reduction of CO2 to methanol by a polyenzymatic system encapsulated in phospholipids-silica nanocapsules.* New Journal of Chemistry, 2013. **37**(11): p. 3721-3730.
19. Liu, W., et al., *Enzyme-catalyzed Sequential Reduction of Carbon Dioxide to Formaldehyde.* Chinese Journal of Chemical Engineering, 2014. **22**(11-12): p. 1328-1332.

20. Kavil, Y.N., et al., *Photocatalytic conversion of CO2 into methanol over Cu-C/TiO2 nanoparticles under UV light and natural sunlight.* Journal of Photochemistry and Photobiology a-Chemistry, 2017. **347**: p. 244-253.
21. Obert, R. and B.C. Dave, *Enzymatic conversion of carbon dioxide to methanol: Enhanced methanol production in silica sol-gel matrices.* Journal of the American Chemical Society, 1999. **121**(51): p. 12192-12193.
22. Das, S. and W.M.A.W. Daud, *Photocatalytic CO2 transformation into fuel: A review on advances in photocatalyst and photoreactor.* Renewable & Sustainable Energy Reviews, 2014. **39**: p. 765-805.
23. Yadav, R.K., et al., *Highly Selective Solar-Driven Methanol from CO2 by a Photocatalyst/Biocatalyst Integrated System.* Journal of the American Chemical Society, 2014. **136**(48): p. 16728-16731.
24. Jhong, H.R., S.C. Ma, and P.J.A. Kenis, *Electrochemical conversion of CO2 to useful chemicals: current status, remaining challenges, and future opportunities.* Current Opinion in Chemical Engineering, 2013. **2**(2): p. 191-199.
25. Sheldon, R.A., *Enzyme immobilization: The quest for optimum performance.* Advanced Synthesis & Catalysis, 2007. **349**(8-9): p. 1289-1307.
26. Mateo, C., et al., *Improvement of enzyme activity, stability and selectivity via immobilization techniques.* Enzyme and Microbial Technology, 2007. **40**(6): p. 1451-1463.
27. Masuda, Y., et al., *Enhancement of cost-effectiveness and activity of formaldehyde dehydrogenase by immobilization onto mesoporous silica with an interparticle pore structure.* Chemistry Letters, 2013. **42**(10): p. 1252-1254.
28. Carlsson, N., et al., *Enzymes immobilized in mesoporous silica: A physical-chemical perspective.* Advances in Colloid and Interface Science, 2014. **205**: p. 339-360.
29. Zhou, Z. and M. Hartmann, *Progress in enzyme immobilization in ordered mesoporous materials and related applications.* Chemical Society Reviews, 2013. **42**(9): p. 3894-3912.
30. Fried, D.I., F.J. Brieler, and M. Froeba, *Designing Inorganic Porous Materials for Enzyme Adsorption and Applications in Biocatalysis.* Chemcatchem, 2013. **5**(4): p. 862-884.
31. Russo, P.A., et al., *Tailoring the surface chemistry of mesocellular foams for protein adsorption.* Colloids and Surfaces a-Physicochemical and Engineering Aspects, 2011. **386**(1-3): p. 25-35.
32. Guilbault, G.G., *Analytical Uses Of Immobilized Enzymes*, in *Enzymology in the Practice of Laboratory Medicine*, P. Blume and E.F. Freier, Editors. 1974, Academic Press. p. 203-228.
33. Nelson, D.L., et al.F, *Lehninger principles of biochemistry*. 2008, New York: W.H. Freeman.
34. Johnson, K.A. and R.S. Goody, *The Original Michaelis Constant: Translation of the 1913 Michaelis–Menten Paper.* Biochemistry, 2011. **50**(39): p. 8264-8269.
35. Kleber, H.-P., *Geoffrey Zubay (Coordinating Author), Biochemistry (Second Edition). XXIX + 1266 S., 946 Abb., 121 Tab. New York—London 1988. Macmillan Publishing Company and Collier Macmillan Publishers. ISBN: 0–02–432080.* Journal of Basic Microbiology, 1990. **30**(5): p. 384-384.
36. Cornish-Bowden, A., *Fundamentals of Enzyme Kinetics*. 2012, Weinheim, GERMANY: John Wiley & Sons, Incorporated.
37. Murzin, D.Y. and T. Salmi, *Chapter 6 - Enzymatic Kinetics*, in *Catalytic Kinetics (Second Edition)*, D.Y. Murzin and T. Salmi, Editors. 2016, Elsevier: Amsterdam. p. 281-343.
38. Labrou, N.E. and D.J. Rigden, *Active-site characterization of Candida boidinii formate dehydrogenase.* Biochemical Journal, 2001. **354**: p. 455-463.
39. Caspi, R., et al., *The MetaCyc database of metabolic pathways and enzymes and the BioCyc collection of pathway/genome databases.* Nucleic Acids Research, 2016. **44**(D1): p. D471-D480.
40. Schirwitz, K., A. Schmidt, and V.S. Lamzin, *High-resolution structures of formate dehydrogenase from Candida boidinii.* Protein Science, 2007. **16**(6): p. 1146-1156.

41. Tanaka, N., et al., *Crystal structure of formaldehyde dehydrogenase from Pseudomonas putida: the structural origin of the tightly bound cofactor in nicotinoprotein dehydrogenases.* Journal of Molecular Biology, 2002. **324**(3): p. 519-533.
42. Luo, J.Q., et al., *Cascade catalysis in membranes with enzyme immobilization for multi-enzymatic conversion of CO2 to methanol.* New Biotechnology, 2015. **32**(3): p. 319-327.
43. Raj, S.B., S. Ramaswamy, and B.V. Plapp, *Yeast Alcohol Dehydrogenase Structure and Catalysis.* Biochemistry, 2014. **53**(36): p. 5791-5803.
44. Ruschig, U., et al., *CO2 Reduction To Formate By Nadh Catalyzed By Formate Dehydrogenase From Pseudomonas-Oxalaticus.* European Journal of Biochemistry, 1976. **70**(2): p. 325-330.
45. Huang, J.H., M. Antonietti, and J. Liu, *Bio-inspired carbon nitride mesoporous spheres for artificial photosynthesis: photocatalytic cofactor regeneration for sustainable enzymatic synthesis.* Journal of Materials Chemistry A, 2014. **2**(21): p. 7686-7693.
46. Jiang, Z.Y., C.Q. Lu, and H. Wu, *Photoregeneration of NADH using carbon-containing TiO2.* Industrial & Engineering Chemistry Research, 2005. **44**(12): p. 4165-4170.
47. Quinto, T., V. Köhler, and T.R. Ward, *Recent Trends in Biomimetic NADH Regeneration.* Topics in Catalysis, 2014. **57**(5): p. 321-331.
48. Ullah, N., I. Ali, and S. Omanovic, *Direct electrocatalytic reduction of coenzyme NAD+ to enzymatically-active 1,4-NADH employing an iridium/ruthenium-oxide electrode.* Materials Chemistry and Physics, 2015. **149-150**: p. 413-417.
49. Weckbecker, A., H. Gröger, and W. Hummel, *Regeneration of Nicotinamide Coenzymes: Principles and Applications for the Synthesis of Chiral Compounds*, in *Biosystems Engineering I: Creating Superior Biocatalysts*, C. Wittmann and R. Krull, Editors. 2010, Springer Berlin Heidelberg: Berlin, Heidelberg. p. 195-242.
50. Huang, J., M. Antonietti, and J. Liu, *Bio-inspired carbon nitride mesoporous spheres for artificial photosynthesis: photocatalytic cofactor regeneration for sustainable enzymatic synthesis.* Journal of Materials Chemistry A, 2014. **2**(21): p. 7686-7693.
51. Vrtis, J.M., et al., *Phosphite Dehydrogenase: A Versatile Cofactor-Regeneration Enzyme.* Angewandte Chemie International Edition, 2002. **41**(17): p. 3257-3259.
52. Shi, Q., et al., *Visible-light photocatalytic regeneration of NADH using P-doped TiO2 nanoparticles.* Journal of Molecular Catalysis B-Enzymatic, 2006. **43**(1-4): p. 44-48.
53. Lagaly, G., *K. K. Unger: Porous Silica — its properties and use as support in column liquid chromatography. Elsevier Scientific Publishing Co., Amsterdam, Oxford, New York 1979. 226*
54. Liu, J., et al., *The bioinspired construction of an ordered carbon nitride array for photocatalytic mediated enzymatic reduction.* Physical Chemistry Chemical Physics, 2014. **16**(28): p. 14699-14705.
55. Kim, J., et al., *Energetics of protein adsorption on amine-functionalized mesostructured cellular foam silica.* Journal of Chromatography A, 2011. **1218**(43): p. 7796-7803.
56. Salimi, A., et al., *Electrocatalytic reduction of NAD+ at glassy carbon electrode modified with single-walled carbon nanotubes and Ru(III) complexes.* Journal of Solid State Electrochemistry, 2009. **13**(3): p. 485-496.
57. Liu, J. and M. Antonietti, *Bio-inspired NADH regeneration by carbon nitride photocatalysis using diatom templates.* Energy & Environmental Science, 2013. **6**(5): p. 1486-1493.
58. Kirk, O., T.V. Borchert, and C.C. Fuglsang, *Industrial enzyme applications.* Current Opinion in Biotechnology, 2002. **13**(4): p. 345-351.
59. Mohamad, N.R., et al., *An overview of technologies for immobilization of enzymes and surface analysis techniques for immobilized enzymes.* Biotechnology & Biotechnological Equipment, 2015. **29**(2): p. 205-220.

60. Tran, D.N. and K.J. Balkus, Jr., *Perspective of Recent Progress in Immobilization of Enzymes.* Acs Catalysis, 2011. **1**(8): p. 956-968.
61. Kuchler, A., et al., *Enzymatic reactions in confined environments.* Nature Nanotechnology, 2016. **11**(5): p. 409-420.
62. Zhang, D.H., L.X. Yuwen, and L.J. Peng, *Parameters Affecting the Performance of Immobilized Enzyme.* Journal of Chemistry, 2013.
63. Talbert, J.N. and J.M. Goddard, *Enzymes on material surfaces.* Colloids and Surfaces B-Biointerfaces, 2012. **93**: p. 8-19.
64. Jia, F., B. Narasimhan, and S. Mallapragada, *Materials-Based Strategies for Multi-Enzyme Immobilization and Co-Localization: A Review.* Biotechnology and Bioengineering, 2014. **111**(2): p. 209-222.
65. Lettow, J.S., et al., *Hexagonal to mesocellular foam phase transition in polymer-templated mesoporous silicas.* Langmuir, 2000. **16**(22): p. 8291-8295.
66. Pierre, A.C., *The sol-gel encapsulation of enzymes.* Biocatalysis and Biotransformation, 2004. **22**(3): p. 145-170.
67. Sheldon, R.A., *Cross-Linked Enzyme Aggregates as Industrial Biocatalysts.* Organic Process Research & Development, 2011. **15**(1): p. 213-223.
68. Gustafsson, H., et al., *Immobilization of lipase from Mucor miehei and Rhizopus oryzae into mesoporous silica-The effect of varied particle size and morphology.* Colloids and Surfaces B-Biointerfaces, 2012. **100**: p. 22-30.
69. Zhang, Y. and H. Hess, *Toward Rational Design of High-efficiency Enzyme Cascades.* ACS Catalysis, 2017. **7**(9): p. 6018-6027.
70. Castellana, M., et al., *Enzyme clustering accelerates processing of intermediates through metabolic channeling.* Nature Biotechnology, 2014. **32**(10): p. 1011-+.
71. Zhang, Y., S. Tsitkov, and H. Hess, *Proximity does not contribute to activity enhancement in the glucose oxidase–horseradish peroxidase cascade.* Nature Communications, 2016. **7**: p. 13982.
72. Bauler, P., et al., *Channeling by Proximity: The Catalytic Advantages of Active Site Colocalization Using Brownian Dynamics.* The Journal of Physical Chemistry Letters, 2010. **1**(9): p. 1332-1335.
73. Wheeldon, I., et al., *Substrate channelling as an approach to cascade reactions.* Nature Chemistry, 2016. **8**(4): p. 299-309.
74. Zhang, Y.H.P., *Substrate channeling and enzyme complexes for biotechnological applications.* Biotechnology Advances, 2011. **29**(6): p. 715-725.
75. Raziah, A.Z., A.R. Junizah, and N. Saifuddin, *Synthesis of Carbon Nanotubes Using Natural Carbon Precursor: Castor Oil*, in *International Conference on Fundamental and Applied Sciences 2012*, B. AriWahjoedi, R. Razali, and M. Narahari, Editors. 2012. p. 564-567.
76. Zhao, D.Y., et al., *Nonionic triblock and star diblock copolymer and oligomeric surfactant syntheses of highly ordered, hydrothermally stable, mesoporous silica structures.* Journal of the American Chemical Society, 1998. **120**(24): p. 6024-6036.
77. Korber, N., *Concepts of Nanochemistry. Von Ludovico Cademartiri und Geoffrey A. Ozin.* Angewandte Chemie, 2010. **122**(20): p. 3483-3484.
78. Takahashi, H., et al., *Catalytic activity in organic solvents and stability of immobilized enzymes depend on the pore size and surface characteristics of mesoporous silica.* Chemistry of Materials, 2000. **12**(11): p. 3301-3305.
79. Tu, J., et al., *Mesoporous Silica Nanoparticles with Large Pores for the Encapsulation and Release of Proteins.* Acs Applied Materials & Interfaces, 2016. **8**(47): p. 32211-32219.
80. Grimaldi, J., et al., *Stability of Proteins on Hydrophilic Surfaces.* Langmuir, 2015. **31**(3): p. 1005-1010.

81. Radhakrishna, M., et al., *Stability of Proteins Inside a Hydrophobic Cavity.* Langmuir, 2013. **29**(28): p. 8922-8928.
82. Fan, J., et al., *Rapid and high-capacity immobilization of enzymes based on mesoporous silicas with controlled morphologies.* Chemical Communications, 2003(17): p. 2140-2141.
83. Schmidt-Winkel, P., et al., *Microemulsion templating of siliceous mesostructured cellular foams with well-defined ultralarge mesopores.* Chemistry of Materials, 2000. **12**(3): p. 686-696.
84. Sridhar, M., et al., *Preparation, characterization and lysozyme immobilization studies on siliceous mesocellular foams: Effect of precursor chemistry on pore size, wall thickness and interpore spacing.* Microporous and Mesoporous Materials, 2014. **190**: p. 215-226.
85. Zhao, D.Y., et al., *Triblock copolymer syntheses of mesoporous silica with periodic 50 to 300 angstrom pores.* Science, 1998. **279**(5350): p. 548-552.
86. Imperor-Clerc, M., P. Davidson, and A. Davidson, *Existence of a microporous corona around the mesopores of silica-based SBA-15 materials templated by triblock copolymers.* Journal of the American Chemical Society, 2000. **122**(48): p. 11925-11933.
87. Gustafsson, H., C. Thorn, and K. Holmberg, *A comparison of lipase and trypsin encapsulated in mesoporous materials with varying pore sizes and pH conditions.* Colloids and Surfaces B-Biointerfaces, 2011. **87**(2): p. 464-471.
88. Wang, X., et al., *Bioinspired Approach to Multienzyme Cascade System Construction for Efficient Carbon Dioxide Reduction.* Acs Catalysis, 2014. **4**(3): p. 962-972.
89. Marques Netto, C.G.C., et al. *Carbon dioxide/methanol conversion cycle based on cascade enzymatic reactions supported on superparamagnetic nanoparticles.* Anais da Academia Brasileira de Ciências, 2018. **90**: p. 593-606.
90. Singh, R.K., et al., *Insights into Cell-Free Conversion of CO2 to Chemicals by a Multienzyme Cascade Reaction.* ACS Catalysis, 2018. **8**(12): p. 11085-11093.
91. Nash, T., *The Colorimetric Estimation Of Formaldehyde By Means Of The Hantzsch Reaction.* Biochemical Journal, 1953. **55**(3): p. 416-421.
92. Lowell, S., et al., *Characterization of Porous Solids and Powders: Surface Area, Pore Size and Density*. 2006: Springer Netherlands.
93. Brunauer, S., P.H. Emmett, and E. Teller, *Adsorption of gases in multimolecular layers.* Journal of the American Chemical Society, 1938. **60**: p. 309-319.
94. Condon, J.B., *Chapter 1 - An Overview of Physisorption*, in *Surface Area and Porosity Determinations by Physisorption*. 2006, Elsevier Science: Amsterdam. p. 1-27.
95. Lukens, W.W., et al., *Evaluating pore sizes in mesoporous materials: A simplified standard adsorption method and a simplified Broekhoff-de Boer method.* Langmuir, 1999. **15**(16): p. 5403-5409.
96. Cohan, L.H., *Sorption Hysteresis and the Vapor Pressure of Concave Surfaces.* Journal of the American Chemical Society, 1938. **60**(2): p. 433-435.
97. Barrett, E.P., L.G. Joyner, and P.P. Halenda, *The Determination of Pore Volume and Area Distributions in Porous Substances. I. Computations from Nitrogen Isotherms.* Journal of the American Chemical Society, 1951. **73**(1): p. 373-380.
98. Barrett, E.P., L.G. Joyner, and P.P. Halenda, *The Determination Of Pore Volume And Area Distributions In Porous Substances .1. Computations From Nitrogen Isotherms.* Journal of the American Chemical Society, 1951. **73**(1): p. 373-380.
99. Pednekar, P.P., et al., *Chapter 23 - Mesoporous silica nanoparticles: a promising multifunctional drug delivery system*, in *Nanostructures for Cancer Therapy*, A. Ficai and A.M. Grumezescu, Editors. 2017, Elsevier. p. 593-621.
100. Reimer, L. and H. Kohl, *Transmission Electron Microscopy: Physics of Image Formation*. 2008: Springer New York.

101. Thompson, J.M.T. and J. Stokes Debbie, *Recent advances in electron imaging, image interpretation and applications: environmental scanning electron microscopy.* Philosophical Transactions of the Royal Society of London. Series A: Mathematical, Physical and Engineering Sciences, 2003. **361**(1813): p. 2771-2787.
102. Zhuravlev, L.T., *The surface chemistry of amorphous silica. Zhuravlev model.* Colloids and Surfaces a-Physicochemical and Engineering Aspects, 2000. **173**(1-3): p. 1-38.
103. Ma, L., F. Yang, and J. Zheng, *Application of fluorescence resonance energy transfer in protein studies.* Journal of molecular structure, 2014. **1077**: p. 87-100.
104. *Energy Transfer*, in *Principles of Fluorescence Spectroscopy*, J.R. Lakowicz, Editor. 2006, Springer US: Boston, MA. p. 443-475.
105. Iqbal, A., et al., *Orientation dependence in fluorescent energy transfer between Cy3 and Cy5 terminally attached to double-stranded nucleic acids.* Proceedings of the National Academy of Sciences, 2008. **105**(32): p. 11176-11181.
106. Nabavi Zadeh, P.S., et al., *A fluorescence spectroscopy assay for real-time monitoring of enzyme immobilization into mesoporous silica particles.* Analytical Biochemistry, 2015. **476**: p. 51-58.
107. *Instrumentation in Gas Chromatography: Edited by J. Krugers, Centrex Publishing Company, Eindhoven, 1968, xi+245 pp., price 83 s.* Analytica Chimica Acta, 1969. **46**(2): p. 323.
108. Janák, J., *Chromatographic Detectors: Design, function, and operation: R.P.W. Scott: Marcel Dekker Inc., New York, 1996; pp: XIV + 514; ISBN 0-8247-9779-5; Price U$ 150.* Journal of Chromatography A, 1997. **761**(1): p. 343-344.
109. Yoshimoto, M., et al., *Preparation of liposome-coupled NADH and evaluation of its affinity toward formate dehydrogenase based on deactivation kinetics of the enzyme.* Colloids and Surfaces B: Biointerfaces, 2013. **109**: p. 40-44.
110. Siegel, L.M. and K.J. Monty, *Determination of molecular weights and frictional ratios of proteins in impure systems by use of gel filtration and density gradient centrifugation. Application to crude preparations of sulfite and hydroxylamine reductases.* Biochimica et Biophysica Acta (BBA) - Biophysics including Photosynthesis, 1966. **112**(2): p. 346-362.
111. Sahibzada, M., *Pd-Promoted Cu/ZnO Catalyst Systems for Methanol Synthesis From CO2/H2.* Chemical Engineering Research and Design, 2000. **78**(7): p. 943-946.